HHS Public Access

Author manuscript

Chem Res Toxicol. Author manuscript; available in PMC 2020 December 31.

Published in final edited form as:

Chem Res Toxicol. 2020 May 18; 33(5): 1145–1162. doi:10.1021/acs.chemrestox.0c00072.

Tissue Specific Fate of Nanomaterials by Advanced Analytical Imaging Techniques - A Review

Uschi M. Graham,
Centers for Disease Control and Prevention, National Institute for Occupational Safety and Health, Cincinnati, Ohio 45213, United States; Pharmaceutical Sciences, University of Kentucky, Lexington, Kentucky 40506, United States

Alan K. Dozier,
Centers for Disease Control and Prevention, National Institute for Occupational Safety and Health, Cincinnati, Ohio 45213, United States

Günter Oberdörster,
School of Medicine and Dentistry, University of Rochester Medical Center, Rochester, New York 14642, United States

Robert A. Yokel,
Pharmaceutical Sciences, University of Kentucky, Lexington, Kentucky 40506, United States

Ramon Molina,
Harvard T.H. Chan School of Public Health, Boston, Massachusetts 02115, United States

Joseph D. Brain,
Harvard T.H. Chan School of Public Health, Boston, Massachusetts 02115, United States

Jayant M. Pinto,
Department of Surgery, The University of Chicago Medicine, Chicago, Illinois 60637, United States

Jennifer Weuve,
School of Public Health, Department of Epidemiology, Boston University, Boston, Massachusetts 02118, United States

David A. Bennett
Department of Neurological Sciences, Rush University Medical Center, Chicago, Illinois 60612, United States

Abstract

A variety of imaging and analytical methods have been developed to study nanoparticles in cells. Each has its benefits, limitations, and varying degrees of expense and difficulties in implementation. High-resolution analytical scanning transmission electron microscopy (HRSTEM) has the unique ability to image local cellular environments adjacent to a nanoparticle

Corresponding Author Uschi M. Graham – graham@topasol.com.

The authors declare no competing financial interest.

Complete contact information is available at: https://pubs.acs.org/10.1021/acs.chemrestox.0c00072

at near atomic resolution and apply analytical tools to these environments such as energy dispersive spectroscopy and electron energy loss spectroscopy. These tools can be used to analyze particle location, translocation and potential reformation, ion dispersion, and in vivo synthesis of second-generation nanoparticles. Such analyses can provide in depth understanding of tissue–particle interactions and effects that are caused by the environmental “invader” nanoparticles. Analytical imaging can also distinguish phases that form due to the transformation of “invader” nanoparticles in contrast to those that are triggered by a response mechanism, including the commonly observed iron biomineralization in the form of ferritin nanoparticles. The analyses can distinguish ion species, crystal phases, and valence of parent nanoparticles and reformed or in vivo synthesized phases throughout the tissue. This article will briefly review the plethora of methods that have been developed over the last 20 years with an emphasis on the state-of-the-art techniques used to image and analyze nanoparticles in cells and highlight the sample preparation necessary for biological thin section observation in a HRSTEM. Specific applications that provide visual and chemical mapping of the local cellular environments surrounding parent nanoparticles and second-generation phases are demonstrated, which will help to identify novel nanoparticle-produced adverse effects and their associated mechanisms.

Graphical Abstract

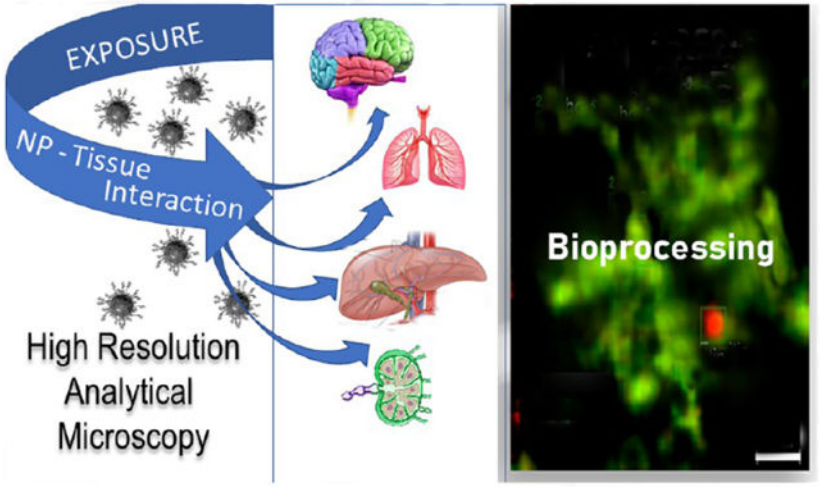

1. INTRODUCTION

Human exposure to nanoparticles (NPs) whether engineered or of environmental origin has been an ongoing concern for decades.[1-8] Nanotechnology is a key modernization driver that balances innovations in NP synthesis with the world’s need and aspiration for novel solutions.[9] There are instances where nanomaterial exposures over long periods of time can result in serious organ injury, chronic disease, and potentially inflict large societal burdens in the form of lost productivity and health costs.[10,11] Case in point, an increased risk for Alzheimer’s and related dementia has been hypothesized to be associated with prolonged exposure to particulate air pollution involving neuronal NP transport from nasal deposits to the central nervous system (CNS) via olfactory and trigeminal pathways.[12] Mounting evidence supports a role for particle–tissue interactions that may promote neurodegeneration

at and beyond the olfactory bulb (OB) and/or brain stem points of CNS entry. To help with these and a host of other health challenges affected by NPs, much effort has been put into expanding existing imaging and analyzing techniques to better explore NPs inside tissues, for example, neurons, axons, and down to subcellular features including mitochondria and the nucleus.

The overarching goal has always been to achieve ever higher analytical and imaging precision to identify and characterize NPs that are trapped inside biological media and avoid tissue breakdown produced by powerful electron beam interactions. This review addresses advanced techniques and the relationship between NP uptake and tissue response that can be (a) scanned and imaged and (b) physiochemically analyzed and quantified at the cellular and subcellular levels. High-resolution electron microscopy analyses are geared toward nondestructive nanoscale data collection. This helps illuminate the dynamic uptake, transformation, breakdown, and reformation processes of NPs inside biological systems. These studies are important where exposure, dose, and cellular NP bioprocessing are related in a nonlinear way. The microscopic thin sections (~50 nm layer), therefore, represent select intermissions that can help describe and interpret the dynamic NP transformations and reformations taking place in vivo over time. Emphasis has always been placed on the precision of the analytical tools when distinguishing between tissue, primary invader nanomaterials, and secondary alteration products. High-resolution scanning transmission electron microscopy (HRSTEM) is the ideal analytical tool to accomplish this task. Conventional low-voltage biological TEM (60–100 keV) was the mainstay for decades in studying cellular ultrastructure and certain disease pathologies and is still important in studying larger (>100 nm) NP cellular interactions and pathology, but on the nanometer and subnanometer scale, HRSTEM has a unique role to play. The study of biologically induced changes either by or to NPs is an area that is quickly expanding and warrants high-resolution analysis coupled with computer programs that aid data collection and evaluation.[13,14]

1.1. Nanoparticle–Tissue Interactions.

Most manufactured nanoparticles (MNPs) range in size from 1 to 100 nm,[15-19] have become an integral part of today’s life, and require safety assessments.[20-26] There is also the relentless influx of anthropogenic pollution-derived NPs from urban settings including industrial and auto exhausts and exposure to nanoplastics which have been linked to major health problems.[16,27,28] Nanosafety studies have seen an exponential rise over the past 20 years, but the threats of NP exposure, for animals, humans, or plants, are still not clearly defined.[29-31] The ultimate fate of NPs in tissues remains unsettled.[10,32,33]

1.2. High-Resolution Analytical Microscopy in Nanotoxicology.

Earlier microscopy techniques employed in biological research could often only partly reveal NPs or recognize their transformations in vitro or in vivo and were only partly able to obtain information about the important underlying adverse effect-inducing mechanisms involved. Central methods include fluorescence, confocal, polarized, and electron microscopy coupled with radiological tracing and measurements of physiologic or toxic response indicators. State- of-the-art material characterization methods with high resolution that are routinely used to identify NPs in the fields of catalysis, electrochemistry, space

technology, semiconductors and other material development fields need to also be considered to characterize NPs inside biological tissues.[34-36] Major microscope manufacturers have a biological-oriented line and a materials-oriented line. Current research, therefore, depends on multidisciplinary collaborations between medical researchers and material scientists. Many techniques have been developed to study NP cellular interactions,[37] but only a dedicated scanning transmission electron microscope has the resolution to image at the near atomic level (HRSTEM or TEM/STEM combination).[14,38] During the last 75 years, TEM has expanded our knowledge about the ultrastructure of cells and tissues. One of the goals has been to characterize structure–function relationships at the cellular and subcellular level.[39] The advancement of "analytical" scopes for biological systems began in the early 1960s and led to the development of energy dispersive spectroscopy (EDS).[40] Since then dramatic improvements have occurred, including the use of electron energy loss spectroscopy (EELS) in biological systems,[37,41,42] which led to ground-breaking research in cellular ultrastructure that is the focus of many ongoing studies,[43-46] including the visualization of unstained DNA nanostructures that can be identified using advanced in-focus phase contrast TEM techniques. A typical HRSTEM used in materials characterization will have EDS and EELS incorporated with the use of computer technology to allow the acquisition of elemental line profiles and maps acquired in STEM mode. This enables not only elemental analysis but also acquisition of material phase changes and oxidative states via the EELS data. In the STEM imaging mode, the beam is focused by the condenser lenses and the objective lens prefield to a point and scanned across the sample in a way like a scanning electron microscope (SEM). The difference is that electrons transmitted through the specimen are imaged using, either or both, a dark- or bright-field detector. Post-magnification of the scattered electrons known as the camera length provides the ability to favor the imaging of light elements versus heavy elements via the dark-field detector. Very large camera lengths or low magnification of scattered electrons results in an imaging condition known as high-angle annular dark-field (HAADF) imaging where the dark-field detector, which is a ring, picks up electrons scattered at high angles. In principle, this imaging mode detects electrons that are not scattered by diffraction but instead scattered by the atomic nucleus. It is sometimes called Z^2 imaging since the brightness will depend upon the radius of the nucleus. This imaging method is particularly useful in detecting heavy atoms in a light matrix material such as metal or metal oxide particles or other heavy NPs in a biological specimen. With computer control of the electron beam in the STEM imaging mode, EDS and EELS signals can be collected simultaneously while scanning. This allows the collection of what is known as spectrum images as either a line profile or a map (examples are shown in section 3). A spectrum image contains either or both a complete EDS and EELS spectrum at each pixel in the line profile or map. These spectrum images can then be analyzed with software to map elements, phase changes, and oxidative states. The combined methods of STEM dark-field imaging, EDS, and EELS are the primary means by which NP location, translocation, their physiochemical characteristics, and their processing in a biological system (NP–tissue interaction) can be studied.

Tissue that is thinned to ~50 nm sections can either be directly visualized in TEM or STEM mode or under cryo-transmission electron microscopy (cryo-TEM). If translocated NPs at the cellular level are agglomerated in larger clusters and strongly absorb the heat from the

high-energy beam, then it would be necessary to use cryo-TEM. Even with the most advanced TEM, great care in sample preparation is critical to preserve the biological structure and preserve the NPs within the cells at their original destination. Therefore, modifications are required for biological specimens to be analyzed in an electron microscope designed for materials characterization for the following reasons: A typical thin section will break apart immediately when subjected to the bright high energy electron beam produced by a field emission electron source operating a 200 keV in TEM imaging mode. Low-electron beam conditions can be used at lower magnification; however, when switching to STEM mode conditions, the beam is abruptly focused to a small high-energy spot. There are several means to stabilize the specimen. Preparation techniques for high-resolution study of macromolecular complexes, organelles within cellular complexes, and translocated NPs are based on meticulous fixation steps, followed by sectioning (~50 nm slices), and then stabilization of the sections onto carbon films. If the sample is still not stable, a carbon film can be evaporated on top of the section on the carbon film grid. Then one must switch to a low-angle dark-field imaging mode to image the biological material (tissue) and locate areas of interest. This is difficult because in a typical STEM the minimum magnification can be 10,000–20,000×. It is advantageous to first identify grid openings of interest in TEM mode and switch back and forth between STEM and TEM imaging modes to find the NPs in structures of interest. The smaller the NPs, the more tedious this process. Once the NPs are located in the STEM imaging mode, the focused beam can induce outgassing from the embedding plastic medium. A cryo-holder can reduce this to minimize or eliminate contamination which corresponds to carbon buildup and deposition in STEM mode. Beam flooding in the low-magnification TEM imaging mode can also reduce contaminates from being deposited in STEM mode. If the contamination being deposited in STEM mode is too great, it can severely limit the ability to use EDS and EELS. The thin sections can be viewed with or without cryo-immobilization. Thicker sections may be cut using a focused ion beam (cryo-FIB), and new hybrid techniques are available to make in situ sectioning possible.

There are some limitations in using the high-resolution STEM technique regarding biological tissues. When searching for particles <10 nm in size with a low spatial density in biological tissue thin sections, it can be very time-consuming to locate a particle. Scope time on expensive instruments can be high and can be a real limitation on what a researcher can accomplish. A skilled operator in advanced STEM analytical techniques with the ability to process and interpret data with at least a basic knowledge of biological structures is required. This represents the need for a multidisciplinary endeavor. Finding a good working partnership can be a limitation. There are also some inherent limitations to the technique. Without cryofixation, diffusible ions and other phenomena at the atomic level can be altered during the fixation process. Also, the intense STEM probe may alter crystal phase states particularly on very small structures. Beam damage is a problem when studying biological molecules, and a variety of methods have been developed to mitigate this problem.[47] STEM resolution is also limited by inelastic electron scattering. This may limit atomic-level resolution, but very small gold clusters of only 11 gold atoms with a diameter of only 0.8 nm have been imaged using a STEM.[48] Effect modulation in thin samples can alter imaging of crystals but tends to be mitigated in biological samples due to inelastic and solvent scattering.[49] Despite these limitations, this is an important and expanding area of research

where new phenomena are being discovered. Eight representative examples are discussed later in Sections 3.1-3.8. Table 1 provides a summary of various analytical imaging techniques. Their capabilities are listed for comparison, but the focus in this review is on HRSTEM use. HRSTEM, coupled with advanced detectors, allows one to probe materials in unparalleled detail, delivering both local chemical information and structural properties. An analytical scope today can image and acquire compositional and electronic information down to the angstrom level.[48] HRSTEM analysis of selected tissues with NPs provides concentration information on certain elements in a two-dimensional (2D) space and also images individual NPs or dispersions that can be resolved at a resolution of down to 0.15 nm (lattice resolution) in an aberration-corrected STEM.[46,48]

The crystal structure of NPs may be analyzed by means of electron diffraction, coupled with chemical fingerprinting of the particles with EDS and EELS analysis and evaluated with the use of dedicated software technology including Gatan Digital Micrograph and Oxford Instruments Aztec to allow the acquisition of elemental line profiles and maps acquired in STEM mode. This allows not only elemental analysis but also acquisition of material phase changes and oxidative states via the EELS data which is of paramount importance when investigating NPs that undergo bioprocessing that results in chemical and structural changes. The EDS and EELS detectors allow the 2D mapping of NPs within a cell. Further, the EELS detector allows differing phases of the parent and daughter grains (i.e., second generation particles) to be distinguished and mapped.[55] Acquisition of material phase changes and oxidative states via EELS data collection[56,57] can then be linked to material phase and spectroscopy databases such as The Materials Project (www.materialsproject.org) and computed from first-principles using spectroscopy-oriented software such as FEFF9,[58] which allows the identification of specific electron excitations between states. STEM mode imaging also provides the ability to distinguish different NPs that are of exogenic and endogenic origins, which is shown in section 3. The common STEM mode of operation to acquire these signals is shown in Figure 1. As an example, high-resolution microscopes have the ability to resolve and image NPs, with the bright- and dark-field detectors in STEM mode operation (Figure 1), and thereby can analyze dispersions of ions (at 0.5% concentration) that were released into the tissue matrix from a parent particle and can identify and analyze the presence of nanometer crystallites that undergo transformations to form 1–2 nm daughter particles at subcellular levels (resolution of ~0.2 nm). Since a nonaberration-corrected field emission electron microscope will typically be able to achieve a STEM spot size of 0.2 nm, tissue-induced changes in NP surfaces versus their core can be analyzed using either spot analysis or trace lines across the particle.[55] These data combined with material phase structure data and spectroscopy computation can, in principle, provide information on chemical, structural, and electronic changes of NPs in tissues.

2. ADVANCED IMAGING AND ANALYSIS OF NANOPARTICLES IN TISSUE SECTIONS

Exposure dose–response relationships in the field of NP toxicity are of paramount importance. This includes detailed characterization of environmental NPs (exposure), tissue retained NPs (dose), and associated cell-tissue-organ responses. It is crucial to gain a more

thorough understanding of NP processing in biological media to be able to make determinations of the long-term toxicological effects after exposure. However, the task is complicated by a lack of information of the physiochemical changes NPs undergo inside cells. Specialized methods of investigation are required. Because of the nano- and subnano-scale dimensions, high-resolution analytical microscopy can be used to monitor the biologically induced NP makeovers both in vitro and in vivo. These studies can provide key insights into relationships between the NPs' synthetic identity and their chemical and biological reactivity,[31,59,60] their biological action as it relates to aggregation and protein interactions including corona formation,[28,61,62] cellular/subcellular bioprocessing, and the physiochemical changes NPs undergo after uptake and translocation.[36] These processes contribute individually and collectively to dose-dependent NP effects.[63] Of course, they will also greatly influence the NPs and their migration, residence time and, ultimately, stability and reactivity in tissues which analytical HRSTEM can help elucidate. A great number of publications focused on the respiratory portal of entry for airborne NPs for designing inhalation studies.[3,4,64] Nonetheless, inhaled NPs after deposition translocate throughout the organism via blood to the organs including liver, spleen, kidney, bones, lymph nodes, intestinal tract, and brain, and studying the NP interactions in these tissues is critical to a deeper understanding of underlying physiological or toxicological outcomes.

Figure 2 illustrates how NP uptake by different organs depends on the type of exposure such as inhalation, injection, dermal, or oral routes. Resultant risk is a function of hazard and exposure, and NP translocation to and retention in different organs needs to be monitored. HRSTEM not only captures the cellular and subcellular interactions and changes NPs undergo, but also informs on the tissue alterations as a function of hazard and exposure.[65] After selection of tissues for the HRSTEM analysis from various harvested organs or cell cultures (tissue sections), it is important that absolutely no staining such as osmication be used in the preparation of thin sections to prevent the interaction of the staining medium with the electron beam. NP uptake into tissue may affect the size, shape, structure, crystallinity, composition (including trace elemental signatures), and valence of the NPs due to tissue interactions. In the case of experimental studies where NPs are available in their original form before exposure, it is important to do an in depth HRSTEM characterization of the starting materials and compare with those that translocated into tissue regions. Differences noted in the material characteristics are due to the in vivo exposure and may be used to interpret the NP transformation after tissue interactions. Bioprocessing of NPs is a step that goes beyond physical translocation of NPs and involves chemical and structural breakdown and biodissolution of NPs inside cells which can be analyzed with HRSTEM. The formation of reaction zones in NPs gives evidence of dynamic changes in the NPs either inward or outward and are telltale signs that particle properties such as composition, density, morphology, crystallinity, or oxidation state were altered. Exogenous NPs are typically affected by a protein corona coating[62] on the NP surface that forms after uptake and during migration. The protein corona may be visualized in HRSTEM if the thickness is >2 nm and helps form a contrast with the surrounding tissue. Since the protein corona has a much lower density than inorganic amorphous or crystalline NPs, it will look more like the organic tissue in appearance and composition, but high-resolution imaging coupled with EDS and EELS mapping may be able to distinguish the fragile interfacial region. This is still a field faced

with great challenges, but the combination of cryo-electron tomography and cryo-HRSTEM can enable ultrastructural analysis of protein aggregates or surface coatings on NPs.

Many NPs are heavily agglomerated after uptake into cells. Agglomerated NPs are more easily located with HRSTEM than their singlets and are typically found inside macrophages. HRSTEM can compare different NPs side-by-side to get a measure of breakdown and transformation reactions or reaction zones. Reactions that cause zonation or partial dissolution of NPs can reveal NP instability inside tissue zones. It may also indicate a cause and effect relationship such as an inflammatory response mechanism. Inflammation in tissues caused by invader NPs and observed in HRSTEM studies has been shown to be accompanied by the formation of numerous ferritins which are biomineralized iron oxy NPs that frequently surround the invader NPs in a halo effect. This represents a combination of exogenic NPs (invader NPs) and endogenic NPs (ferritins surrounding NPs) as illustrated in Figure 2. Ferritins represent a particular type of in vivo generated NPs; more examples are provided in section 3. There are, however, other kinds of in vivo formed NPs that can be directly associated with the invader NPs. These can form when dissolution reactions release ions from disintegrating NPs,[33,55,66] and released ions can become the nutrient supply to nucleate and form secondary NPs;[33,55] examples of secondary NPs are nanoneedles of cerium phosphate that form after the in vivo dissolution of cerium oxide. The secondary NPs may have different size, shape, and surface areas compared with the starting materials. The stability of in vivo formed NPs is different from that of the invader NPs. HRSTEM analysis can map the tissues to identify exogenic versus endogenic NPs and can analyze the redox state of the different particles. When using HRSTEM to look for bioprocessing in different organs and/or different time points, one can gain insights into the stability, reformation, or clearance behavior of the particles. The stability and transformation potential of these NPs are not always the same depending on the host organ.[33,55] NP–tissue interactions, both cellular and subcellular, are a function of the physiological environment, which is limited in its capacity to respond to invader NPs.[31] Smaller NPs (HRSTEM can distinguish NPs as small as 0.5 nm) contribute much higher surface areas per unit mass and, in this regard, yield more reactive surfaces with unique surface properties including charge, composition, structural and chemical variations, redox activities, and catalytic properties. The latter has been expressed as a dose metric in terms of a “specific surface area reactivity”. Since it affects the short and long-term fate of NPs after uptake, HRSTEM studies are required to document particle transformations and interactions and instability signs (dissolution pattern and porosity formation in the NPs) and to look for new phases including recrystallization zones or breakdown products and novel precipitates (Figure 2).

3. NANOPARTICLE–TISSUE INTERACTIONS

The following sections provide specific examples and various NPs after their exposure and translocation to select tissue regions, and the subsequent bioprocessing effects will be discussed. Examples focus either on airborne pollution NPs which represent a wide range of chemistries and sizes, or synthesized NPs with a controlled composition and narrow size range, or in vivo formed NPs that either have a physiological origin (form directly in the cellular environment) and may or may not be linked to the invader NPs after uptake, or originate as secondary NPs after bioprocessing of invader NPs.

3.1. Example I: Ambient Aerosol Nanoparticle Translocation to the CNS.

Atmospheric ultrafine particles (<100 nm) are in the same size category as engineered NPs and can have significant biological activity, including the formation of reactive oxygen species, in cell-free medium as well as in cells. Inhaled NPs can deposit efficiently in all regions of the respiratory tract via diffusion. However, inhaled singlet ~20 nm NPs deposit most efficiently in the alveolar region in humans (close to 50%).[67] It has been shown broadly that NPs translocate, starting from the portal of entry (e.g., the respiratory tract), across cell barriers to secondary organs. From there, NPs can enter cells and disperse into different subcellular structures. However, to reach the CNS and potentially trigger oxidative stress or other adverse effects, NPs potentially can exploit neuronal transport mechanisms via sensory nerves of the nasopharyngeal region, which would allow the NPs to enter the CNS by circumventing the blood–brain barrier. There are two neuronal nose-to-brain pathways: olfactory and trigeminal routes.[68-70] The olfactory system is uniquely suited to provide neuronal transport of inhaled environmental NPs from the nose to the CNS via the olfactory bulb (OB) and is considered a direct pathway for inhaled aerosol constituents to reach the human brain.[75] The trigeminal direct pathway to the brain involves the three branches of the trigeminal nerve which originate in the nasal and oral-pharyngeal tissues entering the right and left trigeminal ganglion close to the brain stem. Although rodent studies confirmed the trigeminal pathway as entry for intranasally administered particles and biologics, trigeminal translocation of particles from nose to brain has been suggested, but has not yet been shown in humans.

The effects of air particulate pollution exposure on impaired olfaction and neurodegeneration were investigated in select cohort studies involving detailed longitudinal studies.[12,71,72] Furthermore, in its recent comprehensive assessment of evidence on particulate matter air pollution exposure, the U.S. Environmental Protection Agency determined that the observed associations of long-term exposure to fine particulate matter air pollution (particles <2.5 mm in aerodynamic diameter) with nervous system outcomes is “likely to be causal”.[73] Initial pilot HRSTEM investigations of human OB tissue sections coupled with EDS and EELS analyses probed the translocation of NPs into OB tissue, measured their corresponding particle size ranges, composition and structure, and compared the results to particulate aerosol constituents in unpublished data. The select study (12 OB thin sections) represented a first step in a series of ongoing investigations. There is a great need to further examine tissue–NP interactions in the OB caused by deposition, transformation, and bioprocessing of pollution particles.

The high-resolution analysis identified both individual NPs and agglomerations in human OB, which is significant since olfactory dysfunction has been shown to habitually predate the development of various impairments of neurodegeneration such as Alzheimer’s Disease. A recent study confirmed that impaired olfaction is associated with cognitive decline and neurodegeneration in the brain.[74] An example of the types and chemistries of translocated NPs inside OB tissues is shown in Figure 3. Collectively, the investigation was able to demonstrate that there are major differences in NPs chemistries, structures, concentrations, and locations within the OB samples. Most frequently amorphous aluminosilicate (Si-Al) NPs and carbon (amorphous carbon; soot) NPs were detected. Heavy-metal inclusions occur

inside both Al-Si and C NPs and are trapped in OB tissue (Figure 3). The heavy metals which frequently included Mn, Zn, Zr, Cr, As, and Pb, among others, were present as discrete nanoinclusions (2–4 nm) dispersed inside larger Si-Al agglomerates. An example of translocated metal NPs in human OB is shown in Figure 3a-g. The ultrastructure of the human OB tissue (imaged at low resolution) with translocated NP (imaged at high resolution) is shown in Figure 3a,b, showing globular ~5–20 μm-sized structures that resemble plaque formation; the globules occur near or next to NPs. Many of the mitochondria in the OB were disrupted, and axons with various degrees of demyelination were found in regions with high concentrations of in vivo formed ferritin NPs (also see later section on Ferritin Nanoparticles) which represent a potential marker for inflammation (Figure 3h-j). The analytical imaging of OB tissue and deeper brain tissue with HRSTEM can help identify novel biomarkers of pollution-derived impairment.[75] Detailed information on the uptake mechanisms of pollution particles and their fate in the OB need to be systematically correlated with subjects that have well-documented impaired olfaction and findings need to be contrasted with those in healthy subjects.

In a related study that focused on myelination with concomitant ultrastructural irregularities following prenatal exposure to ambient concentrated ultrafine particulate matter in a mouse model,[64] HRSTEM investigation coupled with EDS mapping revealed aerosolized NPs translocated to the corpus callosum (Figures 4 and 5) that were imaged immediately juxtaposed to damaged neurons with major demyelination seen in the corresponding high-resolution images marked with arrows. The image resolution was made possible by using a FEI TALOS F200X-STEM that can achieve atomic resolution in both TEM and STEM mode. The high-speed EDS system allowed fast sample scan and elemental mapping which greatly reduces the time the beam is interacting with the sample, thus reducing contamination. In STEM mode, the brighter filament emission gun (FEG) source helps enhance overall image resolution (camera speed 25 frames/s) which results in the detailed structural information seen on the myelin sheets and related damage depicted in Figures 4 and 5 and also allowed fast signal collection without cellular structure damage due to beam interaction. Again, this provided proof of inhaled NP presence in the corpus collosum and was able to identify the chemistries and structures of the NPs as well as significant structural damage as seen by the delamination in the myelin sheets.

3.2. Example II: Nanoplastic–Tissue Interactions.

Micro and nanoplastic particulates are dispersed throughout the environment and pose a significant threat to all life. Fragments of plastic debris smaller than 1 μm cannot be distinguished visually and have raised major concerns about potential interactions with tissues after their uptake. Nanoplastic pollution is not only associated with water bodies (rivers, ocean), but has also been shown to become airborne.[76] The high durability and resistance of plastic polymers to degradation and their high-volume consumption, but low recycling volumes, contributes to the continuous increase of nanoplastics' exposure risks.[28] HRSTEM analysis and EDS mapping of a select human OB section revealed the presence of nanoplastic particulate matter (Figure 6). Nanoplastic–tissue interactions are not known at this time, and this initial finding of nanoplastic debris in the OB indicates that HRSTEM methods can be very useful in helping to identify, characterize, and distinguish nanoplastics

from the host tissue. HRSTEM can further reveal the textures and morphologies of the nanoplastic particles. Moreover, the EDS analysis in Figure 6 shows the elemental signatures are predominantly carbon, nitrogen, and oxygen. There is a recognizable iron peak in the EDS spectrum (Figure 6), suggesting some metal-uptake through adhesion (physical), chemisorption, or metal incorporation during polymer synthesis (catalyst). There is also the potential that the nanoplastic interacted with the tissue and the iron could be due to in vivo formation of ferritin.

Analytical challenges in detecting nanoplastics have been a barrier to their study. It has been suggested recently to synthesize metal-doped nanoplastics to use as standards.[77] The nanoplastic in the OB may have acquired metal contamination which may be helpful in identifying nanoplastics in tissues due to their higher dark-field contrast. HRSTEM coupled with EDS and EELS measurements needs to be applied to studies that develop risk assessment for nanoplastics in animal models, cell culture studies and human case studies.

3.3. Example III: In Vivo Formation of Iron Oxide Nanoparticles in Alveolar Macrophages.

The importance of iron to many physiological outcomes and diseases is well documented. Here we show that iron NPs inside tissue sections can be imaged and distinguished using HRSTEM, EDS, and EELS analysis. The work is a dose and time-controlled rat inhalation study. Amorphous silica was used and effects are described in section 3.6 and involved groups of rats that were exposed to aerosols containing amorphous SiO_2 NPs for 4 h/day, 5 days/week for 4 weeks with a 27 day post-exposure observation period at three concentrations.[36] The subchronic inhalation exposures of the silica NPs were accompanied by in vivo formation of iron oxide NPs inside lung tissue. Tissue sections clearly show that there are two types of iron NPs present and their origin was distinguished as endogenic since no iron oxide NPs were part of the silica aerosol used. Figure 7 shows both types of iron NPs located inside alveolar macrophages. Large agglomerates (up to 400 nm) of iron oxide NPs (Fe_3O_4) occur juxtaposed to much smaller ~5–8 nm $FeHO_2$ NPs (ferritin; oxyhydroxide). This represents different iron NPs with different oxidation states since Fe_3O_4 has a valence of Fe(II) and Fe(III) (mixed valence), while the biomineralized iron in ferritin has a valence of Fe(III). Electron diffraction showed that the Fe_3O_4 NPs have the hexoctahedral ($m3m$) space group and crystallized as a spinel structure (magnetite MG-Fe_3O_4) which has characteristic magnetic properties (Figure 7c-e). The magnetic effects on the tissue are not known at this time. X-ray diffraction analysis is shown in Figure 7d together with the corresponding crystal lattice in Figure 7e. The lattice information obtained by analyzing individual Fe_3O_4 NPs in the alveolar macrophage at high resolution can then be compared with the Materials Genome database (Materials Genome Initiative; www.mgi.gov).

3.4. Example IV: Ferritin Nanoparticles.

The uptake of NPs, either synthesized or from environmental particulate aerosols, results in the partial breakdown and in vivo processing of the invader NPs as imaged and shown in sections 3.1-3.3. Remarkably, there is additional evidence one can gain from HRSTEM: The presence of different invader NPs in different organs (lungs, liver, spleen, brain) after being delivered via different uptake routes (inhalation, intravenous) all share the simultaneous

formation of ferritin NPs that appear in the vicinity of the invader NPs. Ferritins (iron oxyhydroxide, $FeHO_2$) represent biomineralized iron oxy NPs that are typically 5–8 nm and trapped inside the cage of the iron storage protein.[78] Ferritins in tissue thin sections can be analyzed with HRSTEM and are shown to occur within the vicinity of the cell-invading and inflammation-inducing NPs.[79] Moreover, the ferritin NPs are highly concentrated next to the invader NPs when compared to tissue regions that are not affected by inflammation, which can be shown in dark-field STEM images (Figure 8c) and are visualized as solitary bright white spots surrounding invader NPs, each representing one single ferritin NP. A conserved iron binding site, the ferroxidase center of the ferritin protein regulates iron storage in iron metabolism using four channel passages through the protein shell that help facilitate ingress and egress of Fe(II) ions which oxidize and precipitate into an iron core.[80,81] High-resolution imaging as well as spectroscopic and kinetic studies of ferritins are shown in Figures 7 and 8. Although ferritin formational mechanisms have been well documented previously,[80] the spatial association (close locality) of ferritins with invader NPs suggests iron precipitation as a response to the NP uptake. The significance of iron in biological systems is due to its capability to take part in redox reactions. Importantly, this can involve the scavenging of free radicals;[18,79] transferrin receptors at many sites can participate in iron transport at the cellular and subcellular levels. After Fe(II) is oxidized and locked up in the ferric form within the ferritin protein shell, it will no longer participate in free radical formation (Fenton reaction). In fact, the oxidation of one Fe(II) to Fe(III) releases an electron that can neutralize a free radical species and, thereby, act as an antioxidant. It is this catalytic process that gives ferritin NPs their antioxidant property. In the high-resolution dark-field images of tissue thin sections, only the iron oxide core is visible due to the fairly high atomic number and close packing of iron atoms inside the protein cage, while the protein shell has about the same density and general chemical make up as the cellular matrix and there is very little contrast to visualize the protein shell. However, the dense Fe(III) core is ideal for *z*-contrast imaging using HAADF-STEM applications, which demonstrates the presence of ferritin or iron oxyhydroxide ($FeHO_2$) NPs that are typically present throughout cells, but not in the particularly high concentration that is seen with HRSTEM around invader NPs.[36,82] The elevated ferritin NP accumulation (Figure 8a-c) seems independent of the nature of the NPs (environmental particulate matter exposure, nanoplastics, amorphous silica, asbestos fibers, nanotubes, ceria, and others). This would not be known if not for the use of HRSTEM and neither would it be known if just chemically determined Fe, which does not differentiate between endogenous or exogenous Fe, translocated following exposure to airborne environmental iron containing NPs.

3.5. Example V: Nanoceria Bioprocessing.

The first demonstration of NP biotransformation in vivo using HRSTEM or TEM/STEM revealed the dissolution of nanoceria (cerium oxide, CeO_2 NPs) and subsequent formation of second-generation nanoscale particles.[18] Nanoceria is autocatalytically redox active, abrasive, and quite insoluble. Ce (III) predominates on its surface when NPs are <10 nm and Ce(IV) on larger NPs, providing its redox potential. It has industrial applications including as a diesel fuel additive, an abrasive in chemical mechanical planarization in integrated circuit manufacture, as a catalyst in batteries, and as a catalyst structural support. It has been shown to have therapeutic potential at <5 nm to treat many conditions that have an oxidative

stress/inflammation component (see the introduction[66]). Elemental analysis by inductively coupled plasma mass spectrometry demonstrated cerium persistence in 14 organs and two fluids of the rat 90 days after a single nanoceria administration, suggesting prolonged persistence of CeO_2 NPs.[83] However, HRTEM revealed partial dissolution of the ~30 nm ceria NPs in the liver and spleen and the appearance of clouds of 1–3 nm NPs surrounding the ceria NPs. EELS showed the de novo particles to have enhanced Ce(III), providing antioxidant potential. Formation of the 1–3 nm ceria NPs with increased surface Ce(III) was temporally associated with the reversal from pro-oxidant effects seen shortly after nanoceria administration to later antioxidant effects, demonstrating for the first time a fourth stage in the stratified oxidative stress response hierarchical model that heretofore had described three phases of NP-induced adverse biological effects.[84] We suggested that the appearance of the fourth stage was a response to the appearance of the de novo second generation particles, a product of bioprocessing identified by HRTEM (Figure 9). STEM imaging also identified the formation of rod-shaped crystallites in the liver near the bioprocessed CeO_2 NPs (Figures 9 and 10). STEM and EDS revealed they were composed of Ce, O, and P (Figures 9b and 10). Similar cerium phosphate nanoneedles were a product of CeO_2 NP bioprocessing in the spleen of the rats described above,[55] in the liver and spleen of C57BL/6 and BALB/c mice, and in M1- and M2-polarized human and murine macrophages (unpublished results). HRSTEM, TEM/STEM, EELS, and EDS have made possible the appreciation that CeO_2 NPs are not inert particles that persist unaltered in vivo but are bioprocessed to chemical species that have the potential to produce responses different from those produced by the NPs taken up (Figures 9 and 10).

3.6. Example VI: Inhalation of Ionic Species from Aerosols and Subsequent In Vivo Formation of Nanoparticles.

Retention and clearance of NPs in the respiratory tract have been and still are extensively studied, but much less information is available on the formation of NPs from administered ions. The in vivo dissolution of metallic NPs leads to the release of metal ions which can result in the formation of secondary NPs either close by or remotely. There is extensive interest about bioavailable ions, their fate, and potential adverse effects induced by their prolonged persistence.[33,36] The in vivo bioprocessing of CeO_2 NPs was discussed in section 3.5 and bioprocessing of Ce ions is discussed below. The fate of Ce ions after inhalation of $CeCl_3$ aerosols involves a surprisingly long retention of Ce after pulmonary delivery of aerosol $CeCl_3$ in rats.[85] Using HRSTEM, it was found that instillation of $CeCl_3$ transformed to Ce-phosphate nanoneedles in alveolar macrophages (Figure 11). Some needles deposited along cell membrane linings and to a lesser extent inside mitochondria, which is not included in Figure 11. Exactly how the in vivo precipitation of Ce ions formed Ce-phosphate of certain particle sizes, shapes, and structures is still under investigation. Information on the structural characteristics and which cellular regions formed the most secondary NPs from instilled cerium ions was made possible through advanced analytical high-resolution imaging applications. Chemical analysis can determine Ce tissue distribution ($^{141}CeO_2$ in contrast to ionic $^{141}CeCl_3$).[85] Advanced HRTEM can give insights on the specific location of NPs that result from the precipitation of soluble ionic $CeCl_3$ and when coupled with EDS and EELS analyses and was able to demonstrate in vivo formation of Ce-phosphate NPs in the lung after $CeCl_3$ uptake. These combined methods can inform on the slow clearance rate

of soluble ionic $CeCl_3$ and demonstrate some lung retention is directly linked to the conversion of ionic Ce via in vivo precipitation to highly insoluble Ce phosphate NPs (Figure 11).

HRSTEM also informed about the structural, morphological, and chemical signatures of the in vivo formed NPs which represent reaction products from the bioprocessing of instilled ions. Figure 11a,b shows precipitate in lung tissue at increasing magnification settings. Since the precipitated NPs are ~2–5 nm, EELS measurements were obtained using a 1 nm probe (Ce, O, and P edges were investigated). The composition of fine in vivo formed NPs in lungs was verified by identifying EELS signals using a FEI Talos equipped with fast EDS mapping (Figure 11c). Elemental maps generally took 1–2 min to acquire with a sensitivity great enough to detect elemental concentrations in 2 nm-sized particles. Both HRTEM and dark-field STEM demonstrated significant quantities of Ce-phosphate in lysosomal regions (Figure 11e). Higher magnification can show that Ce-phosphate nanoneedles are either part of a larger network that spanned across several hundred nm (Figure 11a,b) or coated the exterior of membrane linings. Select nanoneedles spanned >20 nm in length (Figure 11c). At atomic resolution, it was seen that nanoneedles are composed of individual self-aligned crystallites (Figure 11d). As seen with invader NPs in different exposure outcomes, the uptake of $CeCl_3$ in alveolar tissue also had copious ferritin NPs in the immediate surroundings of the Ce precipitates (Figure 11f). EELS analyses of the ferritin showed a prominent spectrum peak for FeL_3 over FeL_2, which indicates Fe(III) in the individual ferritin NPs. Since $CeCl_3$ ions form Ce-phosphate NPs, the role of “phosphate-rich regions” or intracellular availability of phosphate will need to be addressed to develop formation mechanisms for ion uptake and sequestration as solid particles.

3.7. Example VII: Ostwald Ripening and Particle Growth of Barium Sulfate in Alveolar Macrophages Following Long-Term Exposure.

Site-specific accumulation, retention, and clearance of NPs after inhalation remain a formidable challenge, especially related to the biological activity of NPs. The dissolution and clearance of barium sulfate ($BaSO_4$) NPs after deposition into rat lungs was recently shown to occur at much greater rates than would be expected for a material assumed to be poorly soluble.[33] A 2 year rat inhalation exposure to $BaSO_4$ NPs at a high concentration (50 mg/m^3) resulted in significant $BaSO_4$ accumulation in alveolar macrophages, followed by an early slow buildup in the lungs due to significant $BaSO_4$ dissolution and Ba clearance/biodistribution. After 12–24 months, retention had reached a steady-state lung burden with dense particle crowding inside alveolar macrophages (Figure 12). HRSTEM helped understand the in vivo processing of $BaSO_4$ NPs at the cellular and subcellular levels at various time points, including the initial inhalation stage. Although pulmonary accumulation of NPs occurs gradually, the extensive cumulative retention of $BaSO_4$ NPs in alveolar macrophages suggests early dissolution and subsequent bioprocessing. Since the particle size range inside macrophages at this point was found to be significantly larger (~5–300 nm) compared with the original $BaSO_4$ NPs (~ 40 nm), growth under supersaturation conditions may have resulted in the observed transformation through a process identified as Ostwald ripening, a phenomenon seen in liquid sols. Ostwald ripening is a phenomenon that was not expected to occur inside macrophages.[33] It involves the change of $BaSO_4$ NP structure over

time, whereby the smallest particles with high surface areas per mass dissolve faster. The released Ba and SO_4 ions are in part redeposited onto larger crystals, thereby allowing selective particle growth to take place (Figure 12). This thermodynamically controlled process is driven by the surface properties of larger grains. NPs have comparatively greater numbers of defects per unit surface area compared to macroparticles, and more surface-bound molecules can readily diffuse from NPs into solution. Released Ba and SO_4 ions approach supersaturation conditions via confinement inside the host macrophage, where they condense onto the surfaces of available $BaSO_4$ NPs. When this process continues, it leads to the formation of $BaSO_4$ crystals with well-defined facets (Figure 12). HRSTEM was able to demonstrate how different solubility environments in the lung macrophage can contribute to diverse NP degradation and selective regrowth (Ostwald ripening effect). Taken together, the results help gain a deeper understanding of the bioprocessing that controls the fate of NPs in vivo.

3.8. Example VIII: Amorphous Silica Biotransformation in the Lung.

Analysis of the clearance kinetics of retained lung burden of inhaled amorphous SiO_2 NPs showed significant in vivo solubility, which raises questions about underlying cellular mechanisms that result in the instability of the SiO_2 NPs and related toxicity.[86] Subacute inhalation studies in rats with 30 nm amorphous SiO_2 NPs provided the opportunity to use HRTEM applications and to look for evidence of SiO_2 NP breakdown and mobility in the lung tissue at both cellular and subcellular levels. The principal objective for HRTEM was to examine any nanoscale alteration, dissolution, and processing of SiO_2 NPs in the lung after inhalation by comparing the retained particles with the precursor SiO_2 NPs. This dose and time-controlled inhalation study involved groups of rats that were exposed to aerosols containing amorphous SiO_2 NPs for 4 h/day, 5 days/week for 4 weeks with a 27 day post-exposure observation period at three concentrations. Dose-dependent pulmonary inflammation was induced in the rats, and data were collected in relation to the exposure time and corresponding dose.[36] In this study, subchronic inhalation exposures of the SiO_2 NPs were investigated using an approach of dosimetric particle retention and extrapolation modeling to determine pulmonary clearance rates in rats of these NPs and modeling (extrapolation) to the human lung. Both mechanical particle clearance and partial dissolution of SiO_2 NPs have to be considered as contributing to their clearance. To understand and better characterize the pulmonary dissolution rates, the in vivo bioprocessing mechanism of the particles was examined using HRSTEM/EDS.[36] The results of our advanced high-resolution analytical imaging show the breakdown of SiO_2 in vivo, again confirming the need to use HRSTEM to investigate the subcellular and temporal fate of NPs and how this factors into controlling a response (adverse or benign) after uptake of environmental NPs.

More work is needed to study the dose related effects on the extent of SiO_2 NP breakdown and relocation of Si as a function of saturation levels. Figure 13 is an example of further detailing the chemical and structural content of the Si-rich regions around invader SiO_2 NPs, as shown in the dark-field STEM images that demonstrate a greater extent of in vivo processed SiO_2 NPs in the alveolar macrophage and the development of zone formation.

The chemical breakdown of the SiO_2 NPs (zone I) leads to pitting in the original particles with subsequent material migration and relocation into satellite zones (zone II) which host much smaller particles that are highly dispersed. This is the reason why zone II appears less dense and concentrated in the dark-field STEM image. It will be of paramount importance to apply aberration-corrected STEM and three-dimensional imaging to probe the chemical composition of the matrix of zone II that engulfs the very small SiO_2 NPs.[87] If zone II matrix is chemically distinct from other NP-free regions in the alveolar macrophage that hosts the SiO_2 NPs, it can help determine if protein formation or encapsulation helps stabilize the SiO_2 NPs and make them more biocompatible after in vivo processing. Therefore, long-term exposure to air pollution[88] may need to consider the migration, relocation, and bioprocessing of NPs including amorphous SiO_2 NPs when evaluating trajectories of cognitive decline.

4. SYNOPSIS

The capabilities of high-resolution analytical microscopy (HRSTEM) were demonstrated with examples to show how the inter-relationship between exposure, dose, NP uptake, cellular and subcellular interactions, and effects can be investigated at the nano and subnanometer level. The relationship between dose, particle bioprocessing, and response is an area of active research, as all three may be related in a nonlinear manner. The electron microscope (HRSTEM) probe resolution used in the case studies covered here was at the most 1.7 Å. This resolution has allowed the imaging of the crystal nature, zonation, corona formation, and dissolution pattern of exogenous and endogenous NPs in various tissue regions. With the use of HRSTEM coupled with EDS and EELS capabilities, it is possible to compare size, shape, crystallinity, redox state, and other electronic characteristics of invader NPs and reaction products or secondary NPs including ferritins that form as a result of biologically induced reactions. It is pointed out that relatively insoluble materials like CeO_2 have been observed in vivo to undergo changes far greater than any predictions. This was only revealed during analytical imaging where phase transformations can be recognized that would not be noticed during traditional chemical analysis (ICP-MS). Ionic uptake of Ce in inhalation of $CeCl_3$ was able to be linked to the formation of Ce-phosphate NPs with nearly the same morphology, size, and structure as those formed during the bioprocessing of CeO_2. Because of this, the modeling of dose versus toxicity over time becomes a nonlinear problem because the starting particles can transform over time and initiate different responses that evolve as the dynamic system undergoes further transformations. Thus, the modeling and prediction of dose–response relationships have to take into account highly complex dependencies that need to be characterized using advanced analytical imaging methods like those addressed in this review. Therefore, the long-term goal is to develop multidisciplinary working groups that can address cellular in vitro models and have advanced microscopes for analytical imaging. Greatly improved electron microscopes and associated analytical detectors will provide further insights into both physiological and toxicological phenomena induced by NP–tissue interactions.

ACKNOWLEDGMENTS

This review article is dedicated to the memory of Dr. Patricia Boone, DVM. Advanced microscopy facilities at NIOSH, Cincinnati and at Wright Patterson Air Force Research Laboratory, Dayton were available to U.M.G. and A.K.D. to perform the HRSTEM investigations described in this review.

Funding

The work reported in this publication is partially supported by United States Environmental Protection Agency Science to Achieve Results (grant number RD-833772), National Institute of General Medical Sciences of the National Institutes of Health under award number 1R01GM109195, National Institute on Aging (K23 AG036762), CEFIC-LRI N5 Program, nanoGRAVUR (BMBF, FKZ 03XP0002B), the National Institute of Environmental Health Sciences (P30 ES001247), Nanohealth and Safety Center, New York State, a Boston University Pilot Project, and NSF 1530767. The content is solely the responsibility of the authors and does not necessarily represent the official views of the Environmental Protection Agency, National Institutes of Health, National Institute for Occupational Safety and Health, or Wright Patterson Air Force Research Laboratory.

Biography

Uschi Graham received her B.S. in Chemistry at the University of Heidelberg, Germany and her Ph.D. at Penn State. She has worked at the University of Kentucky in energy research, and her focus has been on catalysis and redox chemistries of nanoparticles after aging. She has used advanced electron microscopy applications to probe catalyst materials and for the past 11 years has used this background to study nanomaterials inside biota, cells, and subcellular structures at UK's Department of Pharmaceutical Sciences and in collaboration with NIOSH (Guest Researcher since 2014) and as Research Director at Faraday Energy.

Dr. Alan Dozier obtained his Ph.D. in physics from Washington University in St. Louis specializing in electron energy loss spectroscopy and scientific computation. He was an instructor at the University of Louisville Medical School Electron Microscopy Facility where he researched cryo-electron microscopy. Currently, he is a Senior Service Fellow at the National Institute of Occupational Safety and Health where he develops new methods of nanoparticle characterization and imaging in electron microscopy.

Dr. Günter Oberdörster received his DVM at the University of Gissen, Germany. He is a Professor Emeritus at the University of Rochester Medical Center where he established an inhalation laboratory for studies of ultrafine particles and effects following inhalation exposure. He has evaluated translocation pathways of inhaled nanosized particles after deposition in the respiratory tract to other organ systems. More recently this includes nanoparticle translocation to the CNS.

Dr. Robert Yokel received his B.S. at the University of Wisconsin-Madison in pharmacy and his Ph.D. at the University of Minnesota in pharmacology. He is currently a Professor in the Department of Pharmaceutical Sciences at the University of Kentucky. His research focus is on nanoparticle uptake, nanotoxicology, and pharmacokinetics. He has used in vivo and in vitro methods to study nanoparticle tissue interactions and bioprocessing phenomena.

Dr. Ramon Molina, D.Sc., DVM is a Senior Research Scientist in the Department of Environmental Health at the Harvard T.H. Chan School of Public Health and Molecular and

Integrated Physiologic Sciences Program. His research focus is on nanotoxicology and nanomedicine.

Dr. Joseph Brain received his S.D. from Harvard T.H. Chan School of Public Health. He is an environmental health researcher who is currently the Cecil K. and Philip Drinker Professor of Environmental Physiology at Harvard T.H. Chan School of Public Health, where he has taught and researched for over 50 years. His research has focused on nanomedicine, nanotoxicology, and public health.

Dr. Jayant Pinto, MD is a Professor of Surgery at the University of Chicago. His research focus has been to understand the effect of aging on sensory disorders and to determine how genetics and the environment modulate susceptibility to these conditions. He has been using this information to develop and test novel treatments by focusing on epidemiology, genomics, public health, and sociology to accomplish these goals.

Dr. Jennifer Weuve, MPH, ScD is an Associate Professor in the Department of Epidemiology of the Boston University School of Public Health (BUSPH). Prior to joining BUSPH, she was on the faculty of the Rush Institute for Healthy Aging in Chicago. In her research, she focuses on issues that accelerate the aging of the brain and body and related health effects of being exposed to environmental toxicants. She serves as a Member-at-Large on the Society for Epidemiologic Research's executive board.

Dr. David Bennett, MD is a faculty at Rush University and is a principal investigator of several studies funded by the National Institute on Aging, including the Rush Alzheimer's Disease Core Center, the Religious Orders Study, and the Rush Memory and Aging Project.

REFERENCES

(1). Elder ACP, Gelein R, Finkelstein JN, Cox C, and Oberdörster G (2000) The pulmonary inflammatory response to inhaled ultrafine particles is modified by age, ozone exposure, and bacterial toxin. Inhalation Toxicol. 12, 227–246.

(2). Oberdörster G, Finkelstein JN, Johnston C, Gelein R, Cox C, Baggs R, and Elder ACP (2000) Acute pulmonary effects of ultrafine particles in rats and mice, pp 1–74, Health Effects Institute, Cambridge, MA.

(3). Maynard AD, Baron PA, Foley M, Shvedova AA, Kisin ER, and Castranova V (2004) Exposure to carbon nanotube material: aerosol release during the handling of unrefined single walled carbon nanotube material. J. Toxicol. Environ. Health, Part A 67 (1), 87–107.

(4). Elder A, Gelein R, Finkelstein JN, Driscoll KE, Harkema J, and Oberdörster G (2005) Effects of subchronically inhaled carbon black in three species. I. Retention kinetics, lung inflammation, and histopathology. Toxicol. Sci 88 (2), 614–629. [PubMed: 16177241]

(5). Rushton EK, Jiang J, Leonard SS, Eberly S, Castranova V, Biswas P, Elder A, Han X, Gelein R, Finkelstein J, and Oberdorster G (2010) Concept of assessing nanoparticle hazards considering nanoparticle dose metric and chemical/biological response metrics. J. Toxicol. Environ. Health, Part A 73 (5), 445–61.

(6). Bonner JC, Silva RM, Taylor AJ, Brown JM, Hilderbrand SC, Castranova V, Porter D, Elder A, Oberdörster G, Harkema J, Bramble L, Kavanagh TJ, Botta D, Nel A, and Pinkerton KE (2013) Interlaboratory evaluation of rodent pulmonary responses to engineered nanomaterials. Environ. Health Perspect 121, 676–682. [PubMed: 23649427]

(7). Sotiriou GA, Watson C, Murdaugh KM, Darrah TH, Pyrgiotakis G, Elder A, Brain JD, and Demokritou P (2014) Engineering safer-by-design silica-coated ZnO nanorods with reduced DNA damage potential. Environ. Sci.: Nano 1 (2), 144–153. [PubMed: 24955241]

(8). Keller J, Wohlleben W, Ma-Hock L, Strauss V, Gröters S, Küttler K, Wiench K, Herden C, Oberdörster G, Van Ravenzwaay B, and Landsiedel R (2014) Time course of lung retention and toxicity of inhaled particles: short-term exposure to nano-ceria. Arch. Toxicol 88 (11), 2033–2059. [PubMed: 25273020]

(9). Bates ME, Keisler JM, Zussblatt NP, Plourde KJ, Wender BA, and Linkov I (2016) Balancing research and funding using value of information and portfolio tools for nanomaterial risk classification. Nat. Nanotechnol 11, 198–203. [PubMed: 26551015]

(10). Nel A, Xia T, Mädler L, and Li N (2006) Toxic potential of materials at the nano level. Science 311, 622–627. [PubMed: 16456071]

(11). Oberdörster G, Oberdörster E, and Oberdörster J (2007) Concepts of nanoparticle dose metric and response metric. Environ. Health Perspect 115 (6), A290–PMC1892118.

(12). Ajmani GS, Suh HH, Wroblewski KE, Kern DW, Schumm P, McClintock MK, Yanosky JD, and Pinto JM (2016) Fine particulate matter exposure and olfactory dysfunction among urban dwelling older US adults. Environ. Res 151, 797–803. [PubMed: 27692900]

(13). Nagashima K, Zheng J, Pamiter D, and Patri AK Biological tissue and cell culture specimen preparation for TEM nanoparticle characterization (2011) Methods in Molecular Biology, Vol. 697, pp 83–91, Humana Press, Totowa, NJ [PubMed: 21116956]

(14). Leapman RD (2008) Nanoscale elemental analysis by EELS in the life sciences. Microsc. Microanal 14, 1378–1379.

(15). Foroozandeh P, and Aziz AA (2015) Merging worlds of nanomaterials and biological environment: factors governing protein corona formation on nanoparticles and its biological consequences. Nanoscale Res. Lett 10, 221. [PubMed: 25995715]

(16). Zhang H, Ji Z, Xia T, Meng H, Low-Kam C, Liu R, Pokhrel S, Lin S, Wang X, Liao YP, Wang M, Li L, Rallo R, Damoiseaux R, Telesca D, Mädler L, Cohen Y, Zink JI, and Nel AE (2012) Use of metal oxide nanoparticle band gap to develop a predictive paradigm for oxidative stress and acute pulmonary inflammation. ACS Nano 6 (5), 4349. [PubMed: 22502734]

(17). Wang W, McCool G, Kapur N, Yuan G, Shan B, Nguyen M, Graham UM, Davis BH, Jacobs G, Cho K, and Hao X (2012) Mixed-phase oxide catalyst based on Mn-mullite (Sm, Gd)Mn_2O_5 for NO oxidation in diesel exhaust. Science 337 (6096), 832–835. [PubMed: 22904009]

(18). Graham UM, Tseng MT, Jasinski JB, Yokel RA, Unrine JM, Davis BH, Dozier AK, Hardas SS, Sultana R, Grulke E, and Butterfield DA (2014) In vivo processing of ceria nanoparticles inside liver: Impact on free radical scavenging activity and oxidative stress. ChemPlusChem 79, 1083–1088. [PubMed: 26322251]

(19). de Souza PM, Rabelo-Neto RC, Borges LEP, Jacobs G, Davis BH, Graham UM, Resasco DE, and Noronha FB (2015) Effect of zirconia morphology on hydrogenation of phenol over Pd/ZrO_2. ACS Catal 5 (12), 7385.

(20). Heinrich U, Fuhst R, Rittinghausen S, Creutzenberg O, Bellmann B, Koch W, and Levsen K (1995) Chronic inhalation exposure of Wistar rats and two different strains of mice to diesel engine exhaust, carbon black, and titanium dioxide. Inhalation Toxicol. 7, 533–556.

(21). Semmler M, Seitz J, Erbe F, Mayer P, Heyder J, Oberdörster G, and Kreyling WG (2004) Longterm clearance kinetics of inhaled ultrafine insoluble iridium particles from the rat lung, including transient translocation into secondary organs. Inhalation Toxicol. 16, 453.

(22). Crosera M, Bovenzi M, Maina G, Adami G, Zanette C, Florio C, and Filon Larese F (2009) Nanoparticle dermal absorption and toxicity: a review of the literature. Int. Arch. Occup. Environ. Health 82 (9), 1043–55. [PubMed: 19705142]

(23). Ravichandran S, Mortensen LJ, and DeLouise LA (2011) Quantification of human skin barrier function and susceptibility to quantum dot skin penetration. Nanotoxicology 5 (4), 675–86. [PubMed: 21142716]

(24). Surekha P, Kishore AS, Srinivas A, Selvam G, Goparaju A, Reddy PN, and Murthy PB (2012) Repeated dose dermal toxicity study of nano zinc oxide with Sprague-Dawley rats. Cutaneous Ocul. Toxicol 31 (1), 26–32.

(25). Mercer RR, Scabilloni JF, Hubbs AF, Wang L, Battelli LA, McKinney W, Castranova V, and Porter DW (2013) Extrapulmonary transport of MWCNT following inhalation exposure. Part. Fibre Toxicol 10, 38. [PubMed: 23927530]

(26). Baisch BL, Corson NM, Wade-Mercer P, Gelein R, Kennell AJ, Oberdörster G, and Elder A (2014) Equivalent titanium dioxide nanoparticle deposition by intratracheal instillation and whole-body inhalation: the effect of dose rate on acute respiratory tract inflammation. Part. Fibre Toxicol 11, 5. [PubMed: 24456852]

(27). Buzea C, Pacheco II, and Robbie K (2007) Nanomaterials and nanoparticles: Sources and toxicity. Biointerphases 2 (4), MR17–MR172. [PubMed: 20419892]

(28). Ribeiro F, O'Brien JW, Galloway T, and Thomas KV (2019) Accumulation and fate of nano-and micro-plastics and associated contaminants in organisms. TrAC, Trends Anal. Chem 111, 139–147.

(29). Burello E, and Worth AP (2011) A theoretical framework for predicting the oxidative stress potential of oxide nanoparticles. Nanotoxicology 5 (2), 228–235. [PubMed: 21609138]

(30). Pan H, Myerson JW, HU L, Marsh JN, Hou K, Scott MJ, Allen JS, Hu G, San Roman S, Lanza GM, Schreiber RD, Schlesinger PH, and Wickline SA (2013) Programmable nanoparticle functionalization for in vivo targeting. FASEB J. 27 (1), 255–264. [PubMed: 23047896]

(31). Krug HF (2014) Nanosafety Research – Are we on the right Track. Angew. Chem., Int. Ed 53 (46), 12304–12319.

(32). Xia T, et al. (2013) Inter-laboratory comparison of in vitro nanotoxicological assays from the NIEHS NanoGo Consortium. Environ. Health Perspect 121, 683–690. [PubMed: 23649538]

(33). Keller JG, Graham UM, Koltermann-Jülly J, et al. (2020) Predicting dissolution and transformation of inhaled nanoparticles in the lung using abiotic flow cells: The case of barium sulfate. Sci. Rep 10, 458. [PubMed: 31949204]

(34). Mühlfeld C, Rothen-Rutishauser B, Vanhecke D, et al. (2007) Visualization and quantitative analysis of nanoparticles in the respiratory tract by transmission electron microscopy. Part. Fibre Toxicol 4, 11. [PubMed: 17996124]

(35). Andrews JC, Meirer F, Liu Y, Mester Z, and Pianetta P (2011) Transmission X-ray microscopy for full-field nano-imaging of biomaterials. Microsc. Res. Tech 74, 671–681. [PubMed: 20734414]

(36). Graham UM, Jacobs G, Yokel RA, Davis BH, Dozier AK, Birch ME, Tseng MT, Oberdörster G, Elder A, and DeLouise L From dose to response: In vivo nanoparticle processing and potential toxicity (2017) in Modelling the Toxicity of Nanoparticles (Tran L, Bañares MA, and Rallo R, Eds.), pp 71–100, Springer, Cham, Switzerland.

(37). Ostrowski A, Nordmeyer DL, Boreham A, et al. (2015) Overview about the localization of nanoparticles in tissue and cellular context by different imaging techniques. Beilstein J. Nanotechnol 6, 263–280. [PubMed: 25671170]

(38). Leapman RD, and Rizzo NW (1999) Toward single atom analysis of biological structures. Ultramicroscopy 78, 251–68. [PubMed: 10389278]

(39). Tomer R, Ye L, Hsueh B, and Deisseroth k (2014) Advanced clarity for rapid and highresolution imaging of intact tissues. Nat. Protoc 9, 1682–1697. [PubMed: 24945384]

(40). Hall TA The history of electron Probe microanalysis in biology (1989) Electron Probe Microanalysis, Applications in Biology and Medicine (Zierhold K, and Hagler HK, Eds.), pp 1–16, Springer-Verlag, Berlin.

(41). Leapman RD Applications of Electron Energy Loss Spectroscopy in Biology: Detection of Calcium (1982) Proceedings of the Electron Microscopy Society of America, pp 412–415, Claitors Press, Baton Rouge, LA.

(42). Aronova MA, and Leapman RD (2012) Development of Electron Energy Loss Spectroscopy in the Biological Sciences. MRS Bull. 37, 53–62. [PubMed: 23049161]

(43). Mielańczyk Ł, Matysiak N, Klymenko O, and Wojnicz R Transmission electron microscopy of biological samples (2015) The Transmission Electron Microscope - Theory and Applications, pp 193–236, InTech, London.

(44). Bryant LH, Kim SJ, Hobson M, Milo B, Kovac ZI, Jikiria N, Lewis BK, Aronov MA, Sousa AA, Zhang G, Leapma RD, and Frank JA (2017) Physicochemical Characterization of Ferumoxytol Heparin and Protamine Nanocomplexes for improved magnetic labeling of stem cells. Nanomedicine 13, 503–513. [PubMed: 27520728]

(45). Kabiri Y, Ravelli RBG, Lehnert T, et al. (2019) Visualization of unstained DNA nanostructures with advanced in-focus phase contrast TEM techniques. Sci. Rep 9, 7218. [PubMed: 31076614]

(46). Pokrovskaya ID, Yadav S, Rao A, McBride E, Kamykowski JA, Zhang G, Aronova MA, Leapman RD, and Storrie B (2020) 3D ultrastructural analysis of α-granule, dense granule, mitochondria, and canalicular system arrangement in resting human platelets. Research and Practice in Thrombosis and Haemostasis. 4, 72–85. [PubMed: 31989087]

(47). Evans JE, Hetherington C, Kirkland A, Chang LY, Stahlberg H, and Browning N (2008) Low-dose aberration corrected cryo-electron microscopy of organic specimens. Ultramicroscopy 108 (12), 1636–1644. [PubMed: 18703285]

(48). Sousa AA, and Leapman RD (2012) Development and Application of STEM for the Biological Sciences. Ultramicroscopy 123, 38–49. [PubMed: 22749213]

(49). Latychevskaia T, and Abrahams JP (2019) Inelastic scattering and solvent scattering reduce dynamical diffraction in biological crystals. Acta Crystallogr., Sect. B: Struct. Sci., Cryst. Eng. Mater 75, 523–531.

(50). Roth GA, Tahiliani S, Neu-Baker NM, and Brenner SA (2015) Hyperspectral microscopy as an analytical tool for nanomaterials. WIREs Nanomed Nanobiotechnol 7, 565–579.

(51). Van Schooneveld MM, Vucic E, Koole R, Zhou Y, Stocks J, Cormode DP, Tang CY, Gordon RE, Nicolay K, Meijerink A, Fayad ZA, and Mulder WJM (2008) Improved biocompatibility and pharmacokinetics of silica nanoparticles by means of a lipid coating: a multimodality investigation. Nano Lett. 8, 2517–2525. [PubMed: 18624389]

(52). Gustafsson MGL (2000) Surpassing the lateral resolution limit by a factor of two using structured illumination microscopy. J. Microsc. (Oxford, U. K.) 198, 82–87.

(53). Chernenko T, Mätthaus C, Milane L, Quintero L, Amiji M, and Diem M (2009) Label-free Raman spectral imaging of intracellular delivery and degradation of polymeric nanoparticle systems. ACS Nano 3, 3552–3559. [PubMed: 19863088]

(54). Sunaoshi T, Kaji K, Orai Y, Schamp CT, and Voelkl E (2016) STEM/SEM, Chemical Analysis, Atomic Resolution and Surface Imaging At ≤ 30 kV with No Aberration Correction for Nanomaterials on Graphene Support. Microsc. Microanal 22, 604.

(55). Graham UM, Yokel RA, Dozier AK, Drummy L, Mahalingam K, Tseng MT, Birch E, and Fernback J (2018) Analytical high-resolution electron microscopy reveals organ specific nanoceria bioprocessing. Toxicol. Pathol 46, 47–61. [PubMed: 29145781]

(56). Muller DA, Sorsch T, Moccio S, Baumann FH, Evans-Lutterodt K, and Timp G (1999) The electronic structure at the atomic scale of ultrathin gate oxides. Nature 399, 758–761.

(57). Egerton RF (2011) Electron Energy Loss in the Electron Microscope, 3rd ed., Springer, New York.

(58). Rehr JJ, Kas JJ, Vila FD, Prange MP, and Jorissen K (2010) Parameter-free calculations of Xray spectra with FEFF9. Phys. Chem. Chem. Phys 12 (21), 5503–5513. [PubMed: 20445945]

(59). Kreyling WG, Semmler-Behnke M, Seitz J, Scymczak W, Wenk A, Mayer P, Takenaka S, and Oberdörster G (2009) Size dependence of the translocation of inhaled iridium and carbon nanoparticle aggregates from the lung of rats to the blood and secondary target organs. Inhalation Toxicol. 21, 55–60.

(60). Kreyling WG, Semmler-Behnke M, Takenaka S, and Moller W (2013) Differences in the Biokinetics of Inhaled Nano-versus Micrometer-Sized Particles. Acc. Chem. Res. 46 (3), 714–722. [PubMed: 22980029]

(61). Docter D, Strieth S, Westmeier D, Hayden O, Gao M, Knauer SK, and Stauber RH (2015) No king without a crown–impact of the nanomaterial-protein corona on nanobiomedicine. Nanomedicine (London, U. K.) 10 (3), 503–19.

(62). Gebauer JS, Malissek M, Simon S, Knauer SK, Maskos M, Stauber RH, Peukert W, and Treuel L (2012) Impact of the nanoparticle-protein corona on colloidal stability and protein structure. Langmuir 28 (25), 9673–9. [PubMed: 22524519]

(63). Walkey CD, and Chan WC (2012) Understanding and controlling the interaction of nanomaterials with proteins in a physiological environment. Chem. Soc. Rev 41 (7), 2780–e99. [PubMed: 22086677]

(64). Klocke C, Sherina V, Graham UM, Gunderson J, Allen JL, Sobolewski M, Blum JL, Zelikoff JT, and Cory-Slechta DA (2018) Enhanced cerebellar myelination with concomitant iron elevation and ultrastructural irregularities following prenatal exposure to ambient particulate matter in the mouse. Inhalation Toxicol. 30 (9–10), 381–396.

(65). Massie I, Dziasko M, Kureshi A, Levis HJ, Morgan L, Neale M, Sheth R, Tovell VE, Vernon AJ, Funderburgh JL, and Daniels JT (2015) Advanced imaging and tissue engineering of the human limbal epithelial stem cell niche. Methods Mol. Biol 1235, 179–202. [PubMed: 25388395]

(66). Yokel RA, Hancock ML, Cherian B, Brooks AJ, Ensor ML, Vekaria HJ, Sullivan PG, and Grulke EA (2019) Simulated biological fluid exposure changes nanoceria's surface properties but not its biological response. Eur. J. Pharm. Biopharm 144, 252–265. [PubMed: 31563633]

(67). Human respiratory model for radiological protection. Ann. ICRP, 1994, 24, 1–300.

(68). Lochhead JJ, and Thorne RG (2012) Intranasal delivery of biologics to the central nervous system. Adv. Drug Delivery Rev 64 (7), 614–628.

(69). Lochhead JJ, Wolak DJ, Pizzo ME, and Thorne RG (2015) Rapid transport within cerebral perivascular spaces underlies widespread tracer distribution in the brain after intranasal administration. J. Cereb. Blood Flow Metab 35 (3), 371–381. [PubMed: 25492117]

(70). Hunter DD, and Dey RD (1998) Identification and neuropeptide content of trigeminal neurons innervating the rat nasal epithelium. Neuroscience 83 (2), 591–599. [PubMed: 9460765]

(71). Weuve J, Puett RC, Schwartz J, Yanosky JD, Laden F, and Grodstein F (2012) Exposure to particulate air pollution and cognitive decline in older woman. Arch. Intern. Med 172 (3), 219–227. [PubMed: 22332151]

(72). Power MC, Adar SD, Yanosky JD, and Weuve J (2016) Exposure to air pollution as a potential contributor to cognitive function, cognitive decline, brain imaging, and dementia: A systematic review of epidemiologic research. NeuroToxicology 56, 235–253. [PubMed: 27328897]

(73). (2019) Integrated Science Assessment (ISA) for Particulate Matter (Final Report), EPA/600/R-19/188, U.S Environmental Protection Agency, Washington, DC.

(74). Dintica CS, Marseglia A, Rizzuto D, Wang R, Seubert J, Arfanakis K, Bennett DA, and Xu W (2019) Impaired olfaction is associated with cognitive decline and neurodegeneration in the brain. Neurology 92 (7), e700–e709. [PubMed: 30651382]

(75). Maher BA, Ahmed IAM, Karloukovski V, MacLaren DA, Foulds PG, Allsop D, Mann DMA, Torres-Jardon R, and Calderon-Garciduenas L (2016) Magnetite pollution particles in the human brain. Proc. Natl. Acad. Sci. U. S. A 113 (39), 10797–10801. [PubMed: 27601646]

(76). Cox KD, Covernton GA, Davies HL, Dower JF, Juanes F, and Dudas SE (2019) Human Comsumption of Microplastics. Environ. Sci. Technol 53 (12), 7068–7074. [PubMed: 31184127]

(77). Mitrano DM, Beltzung A, Frehland S, et al. (2019) Synthesis of metal-doped nanoplastics and their utility to investigate fate and behaviour in complex environmental systems. Nat. Nanotechnol 14, 362–368. [PubMed: 30718833]

(78). Bradley JM, Moore GR, and LeBrun NE (2014) Mechanisms of iron mineralization in ferritins: one size does not fit all. JBIC J. Biol. Inorg. Chem 19 (6), 775–785. [PubMed: 24748222]

(79). Theil EC (2013) Ferritin: the protein nanocage and iron biomineral in health and in disease. Inorg. Chem 52 (21), 12223–12233. [PubMed: 24102308]

(80). Honarmand Ebrahimi K, Bill E, Hagedoorn PL, and Hagen WR (2012) The catalytic center of ferritin regulates iron storage via Fe(II)-Fe(III) displacement. Nat. Chem. Biol 8 (11), 941–948. [PubMed: 23001032]

(81). Tosha T, Behera RK, Ng HL, Bhattasali O, Alber T, and Theil EC (2012) Ferritin protein nanocage ion channels: gating by N-terminal extensions. J. Biol. Chem 287 (16), 13016–13025. [PubMed: 22362775]

(82). Pan Y-H, Sader K, Powell JJ, Bleloch A, Gass M, Trinick J, Warley A, Li A, Brydson R, and Brown A (2009) 3D morphology of the human hepatic ferritin mineral core: New evidence for a subunit structure revealed by single particle analysis of HAADF-STEM images. J. Struct. Biol 166 (1), 22–31. [PubMed: 19116170]

(83). Yokel RA, Au TC, MacPhail RC, Hardas SS, Butterfield DA, Sultana R, Goodman M, Tseng MT, Dan M, Haghnazar SS, Unrine JM, Graham UM, et al. (2012) Distribution, elimination, and

biopersistence to 90 days of a systemically introduced 30 nm ceria engineered nanomaterial in rats. Toxicol. Sci 127 (1), 256–268. [PubMed: 22367688]

(84). Li N, Kim S, Wang M, Froines J, Sioutas C, and Nel A (2002) Use of a stratified oxidative stress model to study the biological effects of ambient concentrated and diesel exhaust particulate matter. Inhalation Toxicol. 14, 459–486.

(85). Molina RM, Konduru NV, Jimenez RJ, Pyrgiotakis G, Demokritou P, Wohlleben W, and Brain JD (2014) Environ. Sci.: Nano 1, 561–573.

(86). Fruijtier-Polloth C (2012) The toxicological mode of action and the safety of synthetic amorphous silica-a nanostructured material. Toxicology 294 (2–3), 61–79. [PubMed: 22349641]

(87). Pennycook SJ, and Varela M (2011) New views of materials through aberration-corrected scanning transmission electron microscopy. Microscopy 60, S213–S223.

(88). Kulick ER, Wellenius GA, Boehme AK, Joyce NR, Schupf N, Kaufman D, Mayeux R, Sacco RL, Manly JJ, and Elkind MSV (2020) Long-term exposure to air pollution and trajectories of cognitive decline among older adults. Neurology 94 (17), e1782–e1792. [PubMed: 32269113]

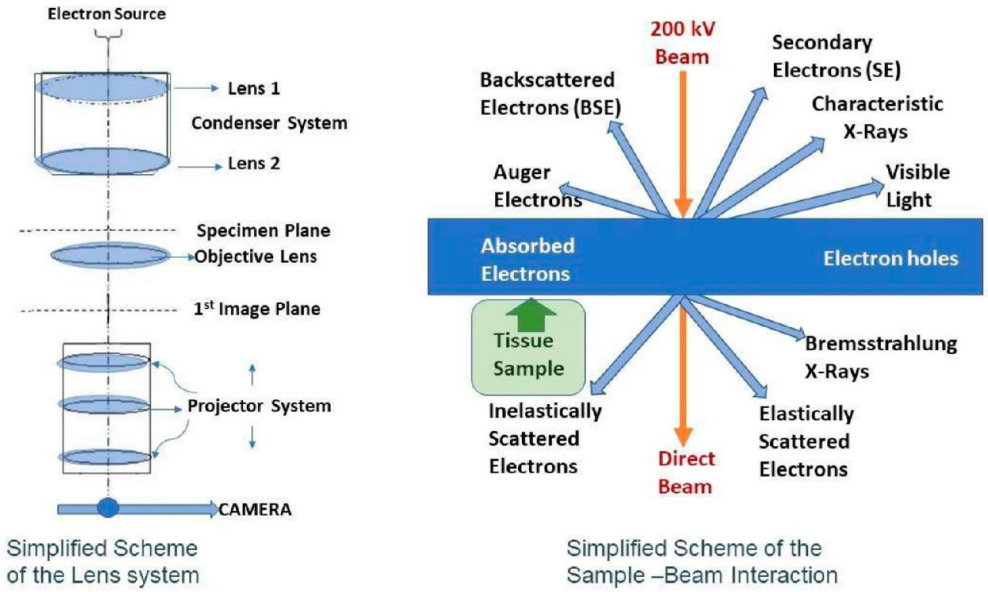

Figure 1.
Schematic HRTEM lens configuration and scheme of sample–beam interactions.

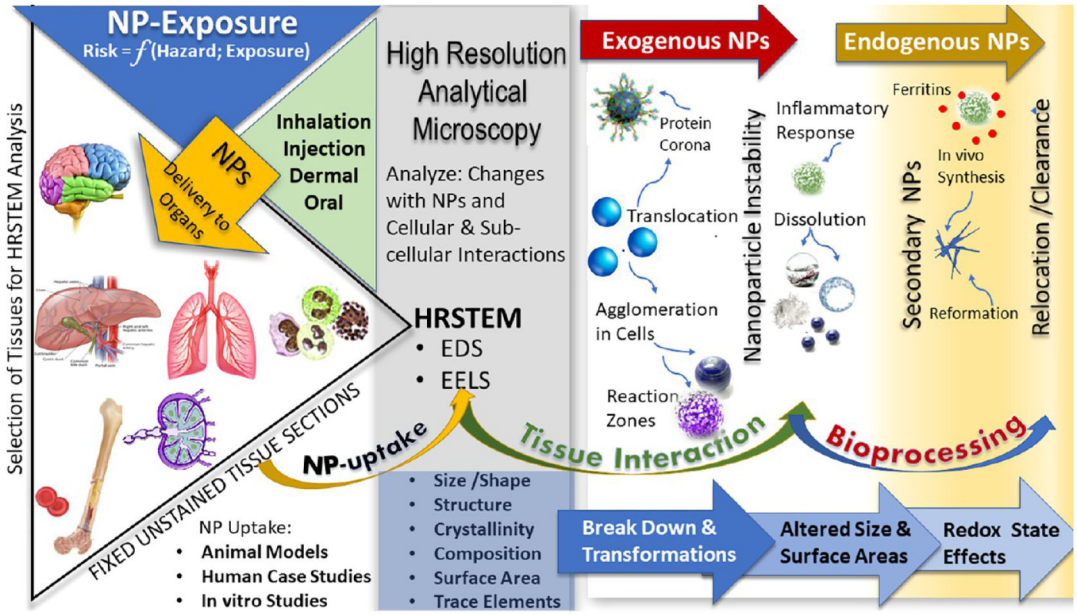

Figure 2.

Schematic of NP uptake and transformations in tissues that can be analyzed using HRSTEM.

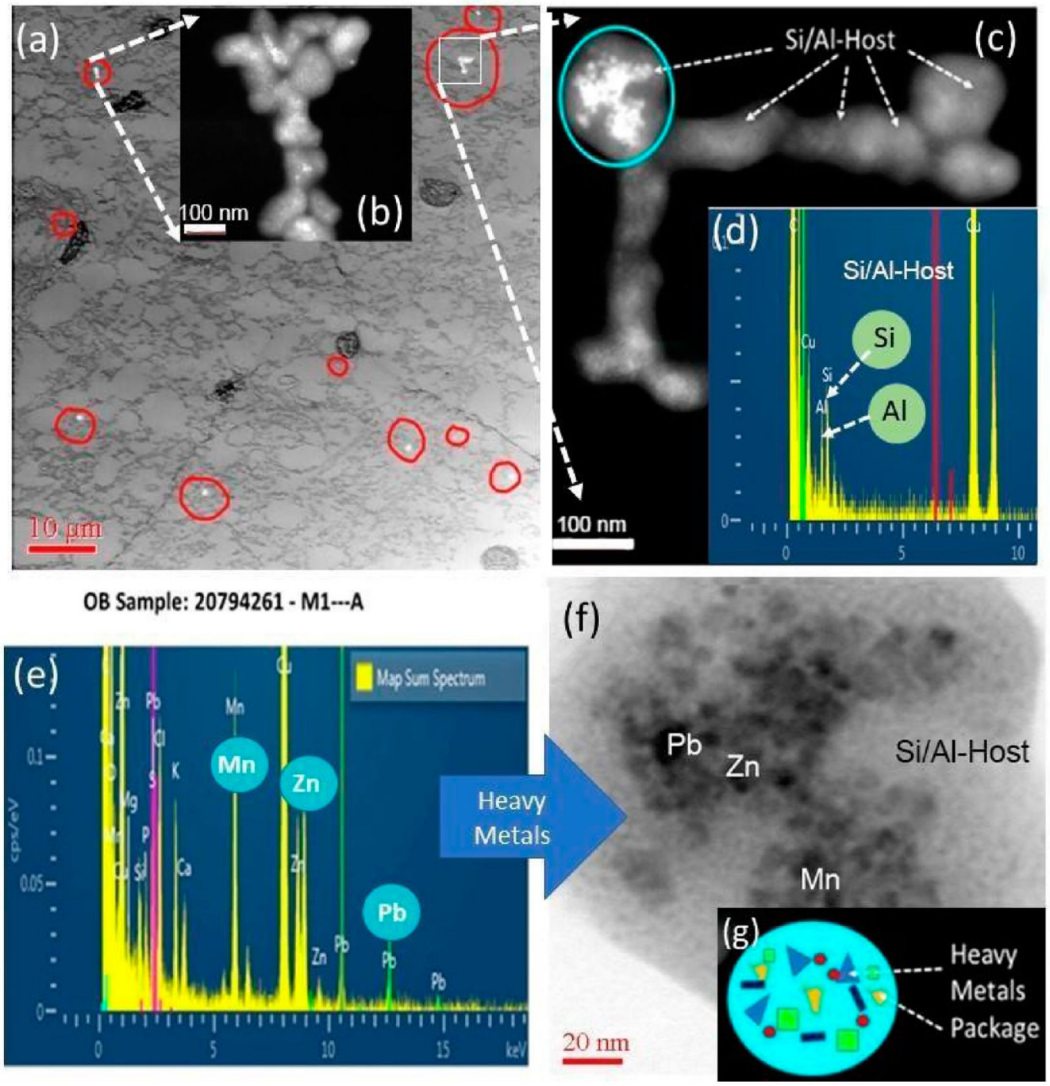

Figure 3.

Nanoparticles in human OB (a) Low-resolution TEM analysis of human OB sample: Ultrastructure of OB tissue with NPs inclusions (white spots within red circles). The dark globular structures are potential plaque formation. Insert (b) illustrates NPs with HRSTEM. (c) HRSTEM of select area with NPs from (a) with EDS spectrum analysis (d) in the NPs identified as Si/Al host particles and the blue circle indicates electron dense particles (metals) inside the Si/Al host. (e) EDS spectrum of the blue circular region containing Mn, Zn, and Pb. (f) HRTEM of the blue circular region with (h) low-resolution STEM analysis of human OB sample; arrow shows area magnified in (i) where ferritin NPs accumulated (white ~5 nm spots). The red squared area shows the region where EDS analysis was taken and is shown in (j) with the presence of Fe.

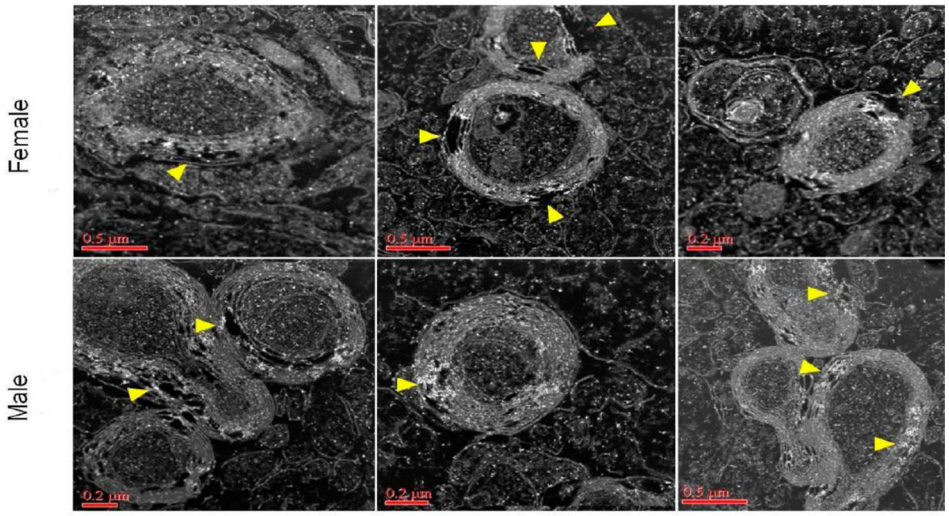

Figure 4.

Corpus callosum from male and female mice after NP exposure. Demyelination with localized iron enrichment shown with Talos (S) STEM analysis. Bright white spots indicate presence of ferritin (iron oxy NPs; confirmed with EELS but not shown here). Yellow arrows mark major regions in the myelin sheets where damage can be seen.

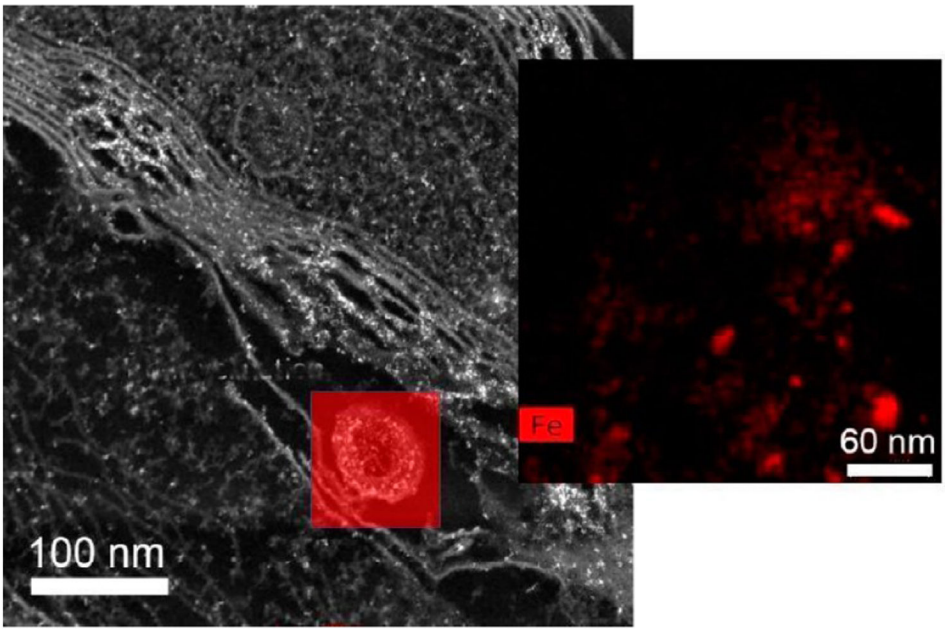

Figure 5.

Demyelination with localized iron enrichment shown with Talos (S) STEM analysis and inset shows EDS mapping (Fe shown in red) taken from red squared area in main image.

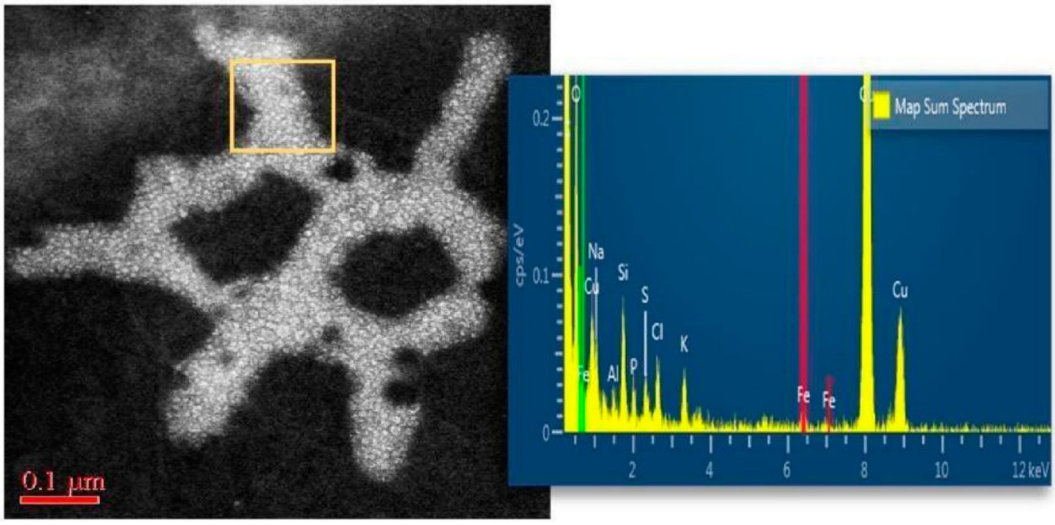

Figure 6.

Nanoplastic particle uptake into human OB illustrated by HRSTEM imaging and EDS elemental mapping taken in the region marked with the yellow square.

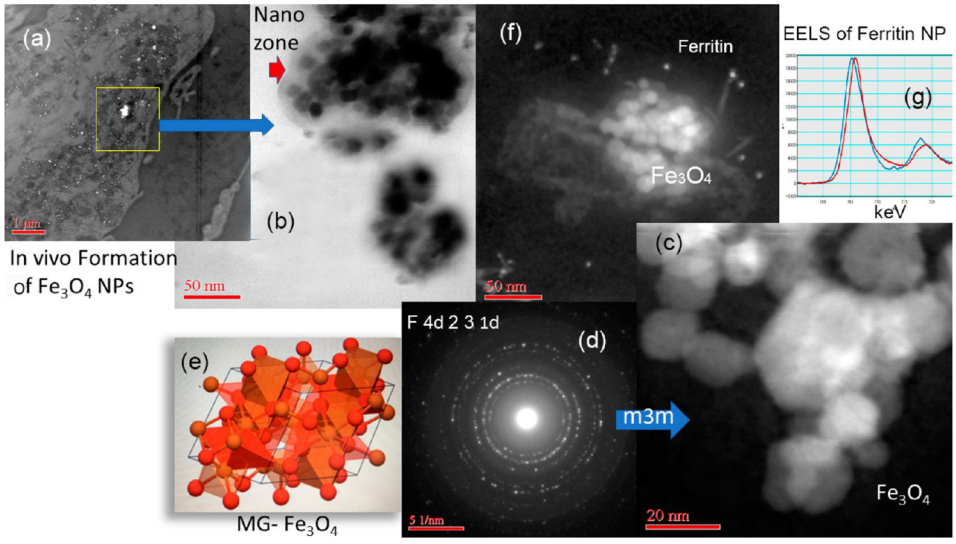

Figure 7.

Endogenous Fe_3O_4 NPs and ferritin NPs inside alveolar macrophage. (a) Low-resolution STEM showing tissue region and NPs (white inclusions). (b) HRSTEM (bright-field detector) showing agglomerated NPs. There is a contrast region between NPs and macrophage “nanozone”. (c) HRSTEM shows agglomerated Fe_3O_4 NPs and (d) is the corresponding X-ray diffraction showing a *m*3*m* crystal structure and (e) compares the in vivo NPs with magnetite (MG)-Fe_3O_4 from a standard (materials genome database). (f) Fe_3O_4 NPs surrounded by smaller ferritin NPs and (g) represents EELS analysis of one ferritin NP shown in (f) with Fe(III).

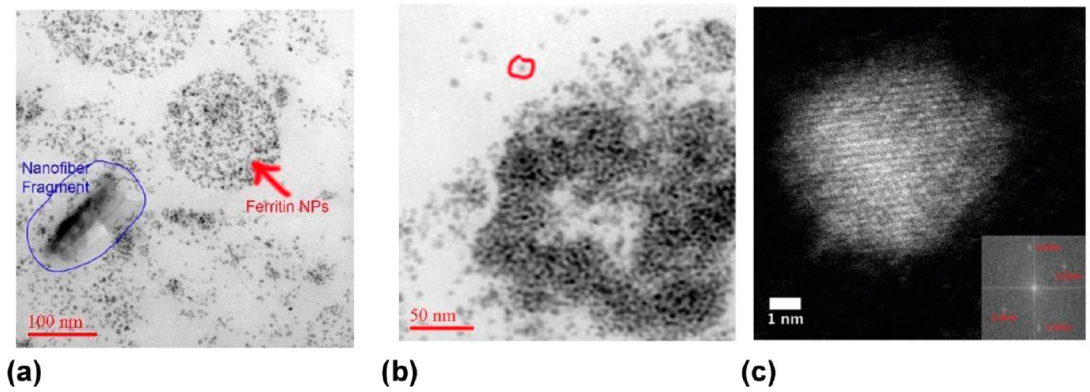

Figure 8.

Ferritin NPs illustrated with a Titan aberration-corrected STEM imaging using a HAADF bright-field detector. (a) Individual ferritin NPs form in the vicinity of an invader nanofiber (from human lung) in macrophages in lung tissue. Ferritins appear to fill entire macrophages. (b) Ferritin NPs appear to form core–shell-type structures and are concentrated inside or around lysosomes. The ferritin NPs ($FeHO_2$) are ~ 5–8 nm, and a singlet particle is indicated by red circle in (b). (c) Fourier transfer of a high-resolution HAADF-STEM image of a ferritin core particle. Measurement of the interplanar spacings shows them to be 0.25 and 0.26 nm.

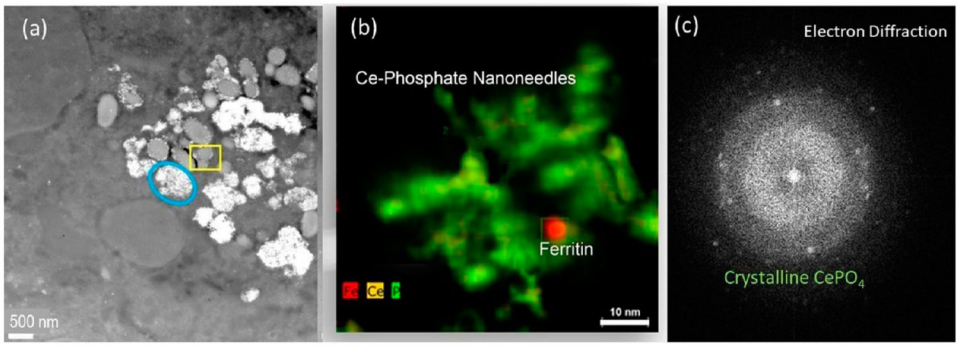

Figure 9.

Talos (S) STEM images of bioprocessed nanoceria in spleen from iv injected rats at 4 weeks post-treatment. (a) The blue oval marks a lysosomal region which is almost filled with NPs. The yellow square indicates a lysosome with minor NP content. (b) Talos elemental mapping (Fe, Ce, P) of the region in the yellow square with Ce-phosphate nanoneedles and a ferritin NP. (c) Electron diffraction of the nanoneedles corresponds to crystalline $CePO_4$.

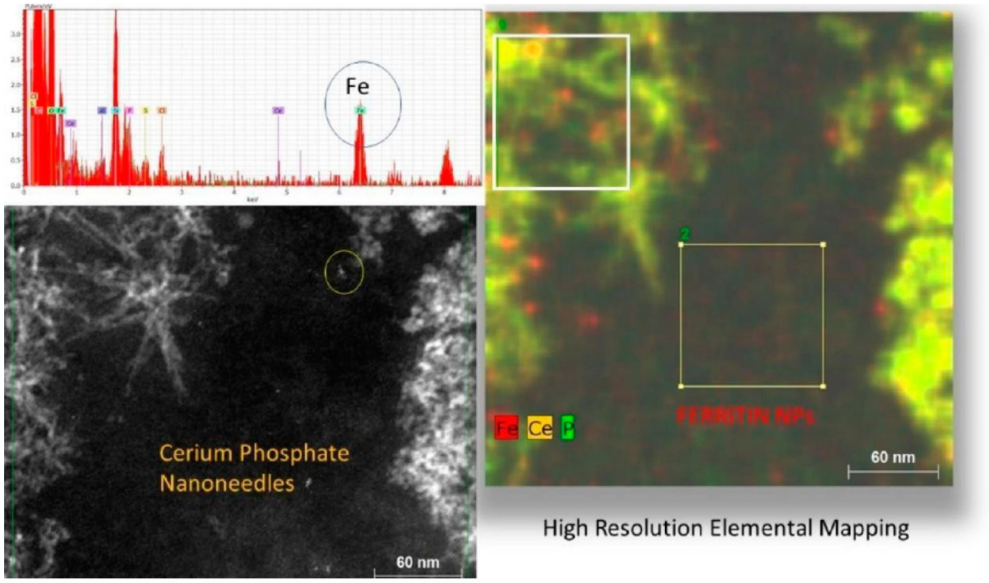

Figure 10.

Accumulation of cerium phosphate nanoneedles inside rat spleen after iv injection of nanoceria. The *z*-contrast imaging using HAADF-STEM (left) and EDS mapping (Fe, Ce, P) of same region with corresponding EDS spectrum taken from the squared areas identifies abundant Fe NPs (ferritin; $FeHO_2$) in the vicinity of invader NPs (CeO_2 and Ce-phosphate nanoneedles). The ferritin NPs are ~5–8 nm.

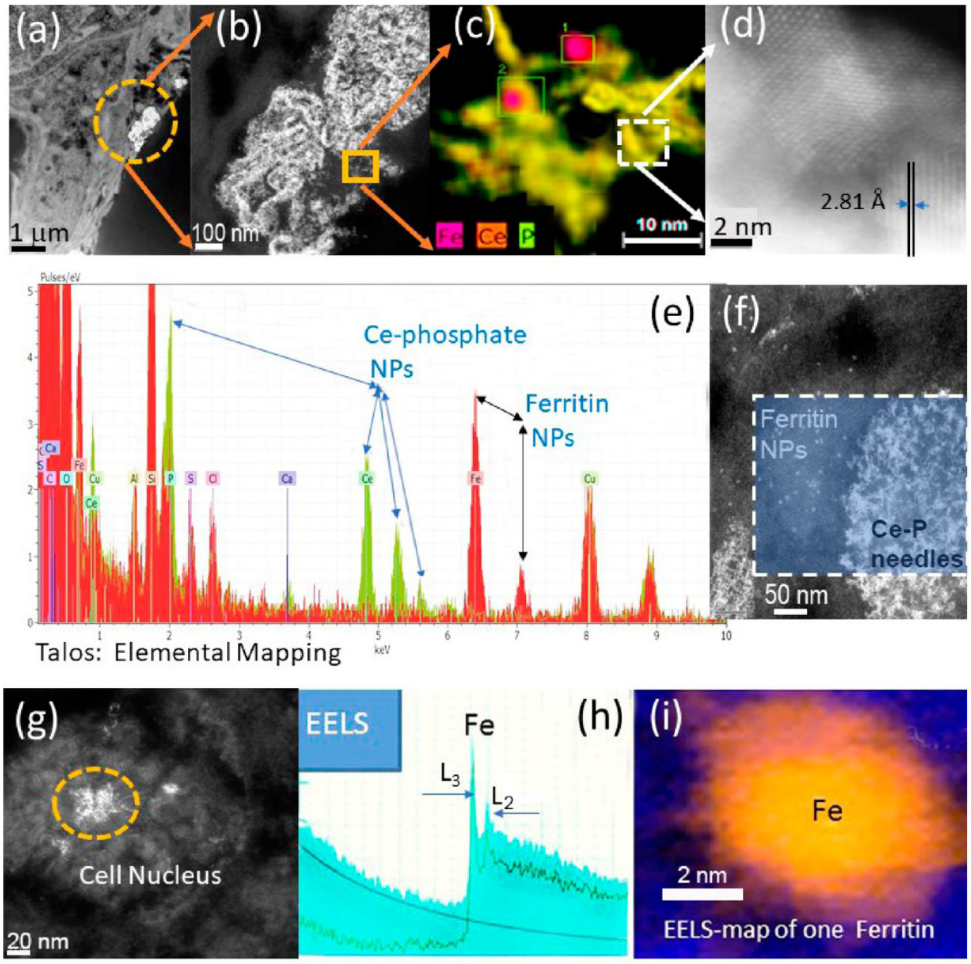

Figure 11.

HRSTEM illustrating formation of Ce NPs in Lung after $CeCl_3$ uptake. (a) STEM showing lung with Ce precipitates (in yellow circle). (b) Talos high-resolution STEM of precipitate marked in (a). (c) EDS mapping of Ce, P, and Fe of needles marked in (b). (d) Atomic resolution of individual Ce-phosphate needles showing crystal lattice structure with *d*-spacings. (e) Talos elemental mapping of Ce-phosphate nanoneedles from squared region marked in (f) and adjacent ferritin region. (g) HRSTEM showing ferritin in cell nucleus. (h and i) EELS analysis and EELS map of ferritin in alveolar macrophage cell nucleus region.

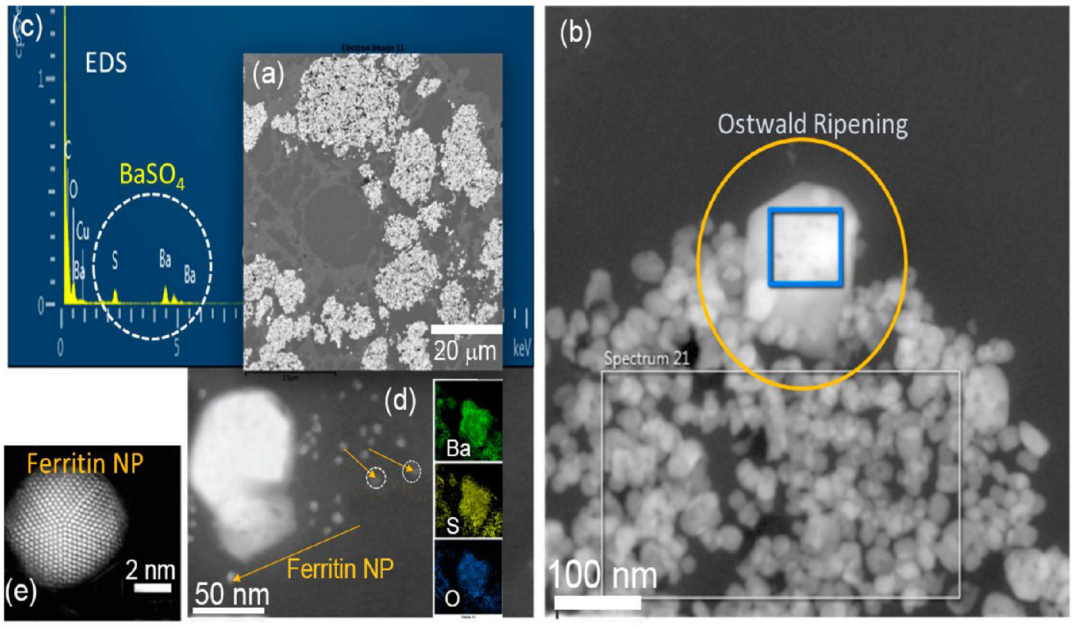

Figure 12.

Barium sulfate uptake by alveolar macrophages after long-term (24 months) exposure and Ostwald ripening effects of the $BaSO_4$ NPs. (a) Low-resolution STEM shows copious macrophages filled with $BaSO_4$ NPs (white areas). (b) Ostwald ripening effect: HRSTEM image with translocated $BaSO_4$ NPs inside a macrophage filled with ~40 nm (or smaller) NPs and a select crystal with significantly larger size and well-defined crystal facets marked with the yellow circle. The blue square inside the large crystal identifies the area that was scanned using EDS analysis. The EDS spectrum shown in (c) identifies Ba and S. (d) HRSTEM of large $BaSO_4$ NP and corresponding EDS maps for Ba, S, and O. The yellow arrows point to ferritin NPs that are in close spatial proximity to the $BaSO_4$ NPs. (e) HAADF-STEM of a single ferritin NP where the ferritin cage is completely crystallized with iron-oxyhydroxide.

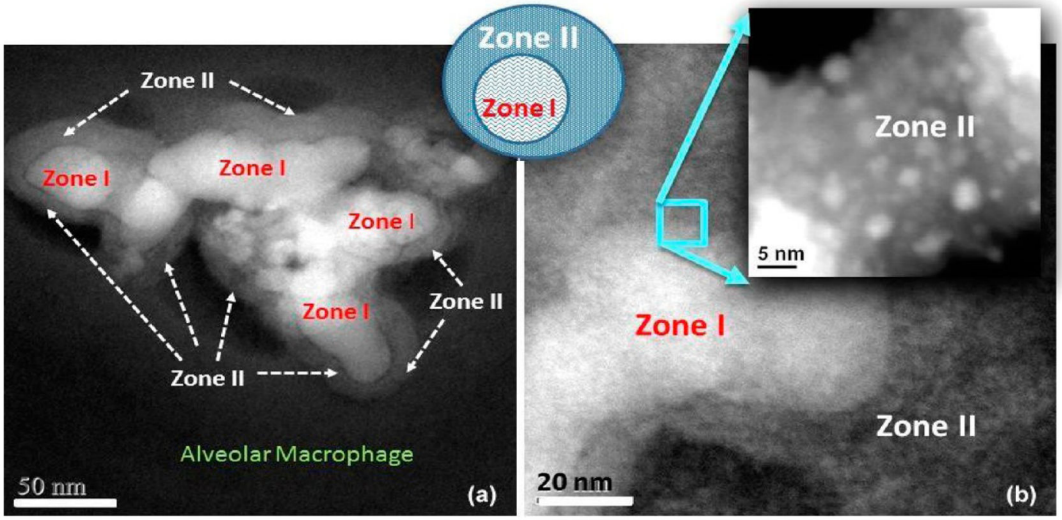

Figure 13.

(a) Dark-field STEM image shows in vivo breakdown of SiO_2 NPs in an alveolar macrophage (zone I) and formation of zone II. (b) Magnified region shows small NPs in zone II.

Table 1.

Summary of Techniques Applied to Nanoparticle Cellular Interaction

technique	type	ability	resolution	ref
hyperspectral microscopy	optical dark-field with very near ir spectroscopy	optical imaging, spectroscopic particle identification	>0.2 nm	50
laser confocal microscopy	optical using scanned laser	specific cell structures (fluorescence) can be singled out along with NP's 3D reconstructions	>0.2 nm	51
super-resolution structured microscopy	high-resolution optical	3D reconstruction, higher resolution than standard optical, can be used on a laser confocal microscope with fluorescent dyes	>0.1 nm	52
Raman microspectroscopy	Raman spectral imaging	Raman spectral mapping combined with optical imaging, can identify particles in some cases	~1 μm	53
soft X-ray microscopy and spectromicroscopy	X-ray imaging, fluorescence, absorption spectroscopy	scanning transmission X-ray microscopy, particle identification using X-ray absorption, X-ray fluorescence, 3D reconstruction, can be done in situ	>10 nm	35
advanced scanning electron microscopy	electron surface imaging, backscatter imaging, STEM imaging, low voltage	SEM, back scatter imaging, bright-field, dark-field, STEM imaging, EDS, EELS spectroscopy, uses low voltages, large field of view, 3D reconstruction	>0.4 nm	54
STEM	electron probe scanned and transmitted through sample, high voltage technique	bright-field, dark-field imaging, EDS and EELS spectroscopy, TEM high-resolution imaging and electron diffraction, 3D reconstruction, cryo-stage	~1 Å	54